THE ASTROPHYSICAL JOURNAL, 359:392–418, 1990 August 20

LARGE PLANETARY NEBULAE AND THEIR SIGNIFICANCE TO THE LATE STAGES OF STELLAR EVOLUTION

JAMES B. KALER[1,2]
Department of Astronomy, University of Illinois
RICHARD A. SHAW[1]
Computer Sciences Corporation, NASA/Goddard Space Flight Center
AND
KAREN B. KWITTER[1]
Department of Astronomy, Williams College
Received 1989 November 20; accepted 1990 February 15

ABSTRACT

We present spectrophotometry of 75 large planetary nebulae, defined here as having Shklovsky radii greater than 0.15 pc. The data are used to calculate nebular parameters and compositions, stellar Zanstra temperatures and luminosities, and core masses. We identify nine new Peimbert type I nebulae (N/O > 0.8, He/H > 0.15), as well as several others with milder enrichments. He/H correlates with N/O much as found before. The scatter of the combined available abundance data suggests that more than one dredge-up scenario is operating in the predecessor stars.

The distribution in core mass, which is heavily dependent upon the uncertain distances, is rather wide. About 40% of the stars that are on cooling tracks are above 0.7 $M_\odot$, and over 15% are above 0.8 $M_\odot$. All the available data on large planetaries demonstrate a clear positive correlation between nitrogen enrichment and core mass (M_c). Mean N/O is constant as M_c increases from 0.55 to 0.8 $M_\odot$, then jumps quickly to values higher than calculated through third dredge-up, providing evidence for some combination of more efficient dredge-up than expected and the existence of hot bottom (envelope) burning. N/O is also anticorrelated with O/H, a relation that becomes apparent only for N/O $\gtrsim$ 1, or $M_c \gtrsim 0.9$. This correlation is difficult to see among the more heavily observed compact nebulae, since (because of evolutionary rates) they tend to have preferentially lower core masses, and consequently lower enrichment factors.

The radii of the nebulae whose stars lie along specific cooling tracks increase monotonically with decreasing central star temperature as expected, giving some credence to the relative Shklovsky distances. For a given central star temperature, the nebular radii also increase with increasing core mass, showing empirically (under the assumption of a common expansion velocity) that in this part of the log L–log T plane the higher mass cores evolve the more slowly in agreement with theoretical prediction. However, theoretical evolutionary rates for the stars of large nebulae appear to be much too slow, predicting nebulae much larger than observed as the stars cool toward the white dwarfs.

Subject headings: nebulae: planetary — spectrophotometry — stars: evolution

I. INTRODUCTION

Large planetary nebulae are of particular significance in the study of the late stages of stellar evolution and in the development of white dwarfs: their electron densities are sufficiently low that the parameter plays little role in the determination of chemical composition; the nebulae tend to be optically thin, so that the simple Shklovsky distance method can be formally applied; the low surface brightnesses of the objects allow a reasonably accurate determination of central star magnitude and hence temperature; and in principle we should be better able to sample planetaries with higher core masses, since their nuclei are predicted to evolve too quickly to be observed easily among the compact nebulae. Two extensive studies of this class of object are available. Kaler (1983, hereafter K83), provided new absolute wide-aperture photometry of major emission lines of 57 large planetaries, and analyzed these observations and those of 25 others with respect to chemical composition and location on the log L–log T plane, central star mass distribution, and mass loss. Kaler and Feibelman (1985) then followed with an examination of the ultraviolet spectra of the nuclei of 32 of them. Here we continue this program with spectrophotometry of 75 planetaries, which includes follow-up observations of 37 of the original K83 sample. We reduce the K83 criterion for "largeness" from a radius of 0.175 pc to 0.15 pc, and with these observations we extend the number of objects studied to 95.

II. THE OBSERVATIONS

We made use of three similar dual-beam instruments: the intensified Reticon scanner (IRS) on the No. 1 0.9 m telescope at Kitt Peak, the intensified image dissector scanner (IIDS) on the Kitt Peak 2.1 m telescope, and the blue Reticon on the University of Arizona Steward Observatory 2.3 m telescope, also located on Kitt Peak. We present a list of the observations in Table 1: the first and second columns give the common names of the nebulae, presented alphabetically, and the Perek-Kohoutek (1967) numbers; the third lists the instrument used,

[1] Visiting Astronomer, Kitt Peak National Observatory, National Optical Astronomy Observatories, operated by Associated Universities for Research in Astronomy, Inc., under contract with the National Science Foundation.
[2] Center for Advanced Study, University of Illinois.

TABLE 1

LIST OF OBSERVATIONS

Nebula	PK No.[a]	Instr.[b]	Date (UT)	Exp[c] (min)	Ap.[d]	Position[e]	λ[f]	Notes
A 1	119+6°1	D	3 Nov 81	32	8	12"S CS	R	
A 2	122-4°1	S	8 Dec 82	18	5	...	B	
A 4	144-15°1	R	14 Oct 80	42	22	whole	...	
A 5	141-7°1	D	3 Nov 81	96	8	N arc	R	
		D	8 Jan 86	48	8	...	B	
		D	11 Jan 86	96	8	...	R	
A 8	167-0°1	R	13 Oct 80	24	22	12"N	...	1
A 9	172+0°1	D	4 Nov 81	64	8	C	R	
A 12	198-6°1	D	4 Nov 81	8	8		R	
A 15	233-16°1	D	4 Nov 81	16	8	CS	R	
		D	4 Nov 81	16	8	15"E CS	R	
A 18	216-0°1	D	9 Jan 86	32	8	...	B	
		D	12 Jan 86	32	8	...	R	
A 19	200+8°1	D	4 Nov 81	24	8	15"N CS	R	
A 20	214+7°1	D	3 Nov 81	20	8	8"N CS	R	
		D	4 Nov 81	16	8	23"S CS	R	
		S	16 Dec 84	19	5	25"W CS	B	
A 33	238+34°1	D	8 Jan 86	24	8	Beam 0	B	
		D	8 Jan 86	24	8	Beam 1	B	
		D	11 Jan 86	32	8	Beam 0	R	
		D	11 Jan 86	32	8	Beam 1	R	
A 36	318+41°1	D	10 Jan 86	64	8	...	B	
		D	11 Jan 86	32	8	...	R	
A 54	55+6°1	D	15 Jun 85	32	8	...	R	
A 59	53+3°1	D	17 Jun 85	8	8	Bt. Patch	B	
		D	18 Jun 85	32	8	in N arc	R	
A 62	47-4°1	S	24 Apr 82	2	5	CS	...	
			24 Apr 82	2	5	25"W CS	...	
A 69	76+1°1	D	4 Nov 81	48	8	SE ring	R	1
A 70	38-25°1	R	14 Oct 80	48	22	C	...	
A 72	59-18°1	D	3 Nov 81	16	8	10"NW CS	R	
A 75	101+8°1	D	3 Nov 81	16	8	3"N CS	R	
		D	3 Nov 81	8	8	6"S CS	R	
A 80	102-5°1	D	18 Jun 85	16	8	E. arc	R	
A 82	114-4°1	D	10 Sep 83	12	8	Bt. star	B	
		D	14 Sep 83	8	8	NW	R	
A 84	112-10°1	R	16 Oct 80	12*	22	A 45"E CS	...	1
		R	16 Oct 80	12*	22	B 45"W CS	...	
Ba 1	171-25°1	D	4 Nov 81	32	8	CS	R	
		D	4 Nov 81	16	8	W ring	R	
		S	29 Oct 83	16	5	CS	B	
DHW 1	228-22°1	D	8 Jan 86	8	8		B	2
= LoTr 1		D	11 Jan 86	48	8	...	R	
He 1-6	65-5°1	D	14 Jan 85	16	8	C	R	
IC 5148	2-52°1	D	4 Nov 81	16	8	30"N CS	R	
Jn	104-29°1	R	13 Oct 80	30*	22	S arc	...	3
		R	13 Oct 80	30*	22	S arc	...	
K1-1	252+4°1	D	13 Jan 86	64	8	...	R	
= A 27								
K1-3	346+12°1	S	2 Jul 81	8*	5	N ring	...	4
= A 38		~		8*	5	N ring	...	
K1-7	197-14°1	R	14 Oct 80	24	22	...	...	
= A 10								
K1-8	223-2°1	D	4 Nov 81	40	8	14"SE CS	...	
K1-9	219+1°1	D	13 Jan 86	48	8	...	R	
K1-13	224+15°1	D	10 Jan 86	64	8	...	B	
= A 25		D	11 Jan 86	48	8	...	R	
K1-14	45+24°1	R	13 Oct 80	32	22	6"S CS	...	5
K1-17	51+6°1	D	4 Nov 81	32	8	13"N CS	R	
K1-20	110-12°1	R	16 Oct 80	48	22	C	...	
K1-22	283+25°1	D	8 Jan 86	16*	8	...	B	6
			13 Jan 86	24*	8	...	R	
K3-27	61+8°1	R	16 Oct 80	32	22	C	...	
K3-73	84+9°1	S	25 Aug 85	16	5	C	...	7
K3-74	78+5°1	S	23 Aug 85	16	5	C	...	7
K3-86	106-4°1	D	14 Sep 83	8	8	C	R	7
		S	22 Jan 87		8	C	...	

TABLE 1—*Continued*

Nebula	PK No.[a]	Instr.[b]	Date (UT)	Exp[c] (min)	Ap.[d]	Position[e]	λ[f]	Notes
K3-91	129+4°1	D	3 Nov 81	12	8	W	R	7
		S	23 Jan 87		8	W		
K3-92	130-3°1	D	3 Nov 81	32	8	W	R	7
		S	4 Dec 86	20	5	C	...	
Lo 4	274+9°1	D	9 Jan 86	32	8	...	B	8
		D	12 Jan 86	64	8	...	R	
LoTr 5		D	12 Jan 86	64	8	...	R	2
M2-51	103+0°1	S	17 Dec 84	16*	5	CS	...	
		D	12 Jan 86	16	8	...	...	
M2-53	104-1°1	D	4 Nov 81	8	8	CS	R	
		S	26 Aug 84	12	5	CS	B	
M2-55	116+8°1	S	22 Jan 87	8	8	C	...	
		S	22 Jan 87	4*	8	E Lobe	...	
		S	22 Jan 86	4*	8	W Lobe	...	
M3-2	240-7°1	D	9 Jan 86	16	8	C	B	
		D	12 Jan 86	8	8	C	R	
M3-3	221+5°1	D	9 Jan 86	16	8	C	B	
		D	11 Jan 86	16	8	C	R	
M4-11	24-5°1	D	18 Jun 85	16	8	C	R	
NGC 246	118-74°1	R	14 Oct 80	32*	22	1′ NCS	...	3
			14 Oct 80	32*	22	...	...	
NGC 650	130-10°1	S	27 Aug 84	8*	5	CS	B	
		S	27 Aug 84	8*	5	25"W CS	B	
NGC 1360	220-53°1	R	16 Oct 80	6*	22	47"N CS	...	1,3
				6*	22		...	
NGC 2438	231-4°2	S	17 Dec 84	14*	5	CS	B	
		S	17 Dec 84	14*	5	25"W CS	B	
NGC 3587	148+57°1	S	16 Dec 84	4*	5	25"W CS	B	9
NGC 4361	294+43°1	D	13 Jun 85	16	8	...	R	
		D	14 Jun 85	16	8	...	B	
NGC 6026	341+13°1	D	13 Jun 85	16	8	CS	R	
		D	14 Jun 85	16	8	CS	B	
NGC 6072	342+10°1	D	28 Jun 84	12	8	N blob	R	
NGC 6781	41-2°1	R	16 Oct 80	12*	22	30"S	...	3
				12*	22		...	
NGC 6842	65+0°1	R	16 Oct 80	24	22	C	...	
NGC 7094	66-28°1	R	13 Oct 80	60	22	34"N CS	...	1
		D	3 Nov 81	4	8	8"N CS	R	
		D	3 Nov 81	4	8	5"S CS	R	
NGC 7139	104+7°1	R	13 Oct 80	16	22	24"N CS	...	
		S	17 Dec 84	17*	5	CS	B	
		S	17 Dec 84	17*	5	25"W CS	B	
NGC 7293	36-57°1	D	3 Nov 81	4*	8	knot	R	
		D	3 Nov 81	4*	8	100"E knot	R	
PC 21	13-7°1	D	10 Sep 83	40	8	C	B	
Pu 1	181+1°1	D	10 Jan 86	32	8	...	B	10
		D	12 Jan 86	32	8	...	R	
PW 1	158+17°1	D	12 Jan 86	64	8*	...	R	11
Shl-89	89-0°1	D	10 Sep 83	20	8	C	B	
		D	12 Jan 86	32	8	C	R	
VV1-2	151+2°1	D	13 Jan 86	16	8	...	R	
VV1-4	197-2°1	S	8 Dec 82	12	5	...	...	
We 1	121+3°1	D	14 Sep 83	16	8	C	B	12
We 2	160-0°1	D	9 Jan 86	32	8	...	B	12
		D	11 Jan 86	64	8	...	R	
We 3	163-0°1	D	9 Jan 86	32	8	...	B	12
		D	12 Jan 86	64	8		R	
We 5	216-4°1	S	22 Jan 87	16	8	...	...	12

NOTES.—(1) Scattered clouds and/or fog; (2) Dengel, Hartl, and Weinberger 1980 and/or Longmore and Tritton 1980; (3) 90″ separation; (4) 25″ separation; (5) spectrum badly confused by bright companion to CS; (6) Kohoutek 1971; (7) Kohoutek 1972; (8) Longmore 1977; (9) CS data not used; (10) Purgathofer 1978; (11) Purgathofer and Weinberger 1980; (12) Weinberger 1977.

[a] Perek and Kohoutek 1967 designation.

[b] D: IIDS; R: IRS; S: Steward Reticon.

[c] Asterisks denote nebular option.

[d] Numbers are aperture diameters in arcseconds.

[e] CS denotes central star, 15″ ECS means 15″ east of the central star, and so on; C means "center"; W means "whole object."

[f] B and R refer to blue and red spectral regions; see data tables for exact coverage. If the column is blank, the full spectrum (3727–6731 Å) was covered by the instrument.

where D R, and S represent the IIDS, IRS, and Steward Reticon, respectively; the next three columns then show the UT dates of the exposures, the exposure times in minutes (Exp), and the diameters of the spectrograph entrance apertures employed (Ap, in arcseconds); the seventh column provides information on the positions observed in the nebulae (see footnote e for a brief explanation); and the last two list the wavelength regions observed, where R and B mean "red" and "blue," respectively, and references to notes. The notes provide the citations to recently discovered objects. Almost all the planetaries were observed with the usual beam-switching procedure. A few were larger than the aperture separation, and were observed in "nebular mode," for which there will ordinarily be two sets of data: these are denoted by asterisks in the "exposure" column; also see the remarks.

The different instruments cover different wavelength regions. The IRS spanned the spectral range of interest, 3700–6800 Å, at about 15 Å resolution, in order to include both the [O II] and [S II] doublets. The IIDS gratings, which gave about 10 Å resolution, were set to cover separately either the red (*R*) portion of the spectrum (4650–6800 Å), or the blue (*B*) (3400–5400 Å). The spectral coverage and resolution provided by the Steward Reticon depended on which of two gratings was selected: For some runs we included only the blue (resolution 4 Å), for others the entire range (resolution 8 Å). If the full range of wavelengths was observed (both *B* and *R*), the "λ" column in Table 1 is blank. We calibrated the data with observations of stars taken from the KPNO IIDS Standard Star Manual (Oke 1974; Stone 1977), and reduced them with standard software available at Kitt Peak and Steward Observatory.

a) Nebulae

We derived nebular line fluxes from the data by fitting Gaussian line profiles via SPEC, a software package developed by University of Illinois graduate students. The program can fit up to four Gaussians at a time, can constrain line widths, and is especially useful for the deconvolution of blends (see Kaler 1985*a* for further description).

The Steward data presented a special problem. All were acquired with first-order spectra. The Reticon is so blue-sensitive that it is affected by the residual second-order ultraviolet light that is passed by the UV 36 order separation filter. Consequently, the standard star data can be considerably in error longward of 6000 Å. We corrected for this effect first by extrapolating the wavelength-dependent corrections (telescope transmission function, atmospheric extinction, and so on) in the affected part of the red spectrum. We then corrected the red emission-line data night by night by either (1) comparing Hα/Hβ flux ratios of Steward data with IIDS data acquired for one or more objects in common or (2) determining expected Hα/Hβ flux ratios from the interstellar extinction found from Hγ and Hδ (see below) and comparing them with the values derived from the initial reductions. The other red lines are close to Hα and were then scaled by the same factors.

We present the relative line fluxes in Tables 2–6, with the exceptions of DHW 1 and LoTr 5, on the usual scale $I(\mathrm{H}\beta) = 100$, *uncorrected for interstellar extinction.* The final results are heterogeneous and depend very much on the surface brightnesses of the nebulae. For some objects we observed a large number of lines (up to nearly 40), for others only a few, which gives us a problem in data presentation. To solve it, we divide the nebulae by their common names, since a particular discovery sequence will usually involve a certain type of object. We consequently list the Abell and Kohoutek nebulae in Tables 2 and 3, respectively; Minkowski objects (with one Peimbert-Costero nebula) in Table 4; and the NGC nebulae in Table 5. Table 6 covers the remainder, presented alphabetically. In each table, the wavelengths and identifications are given in the first two columns.

Most spectral regions of most objects were observed only once, so there is little information on which to base errors, which will be dominated by external effects that are not directly derivable. However, in several cases we observed a nebula with more than one instrument (which provides the red correction mentioned above) or with the same instrument on different nights. Where the data overlap (which may only include a short span common to both *B* and *R* data), we can derive an "error" that is merely the mean value minus one of the two individual measurements. The average of all these values gives a sense of the real typical error, which is $\pm 7\%$ for the brightest lines ([O III] $\lambda\lambda$4959, 50007) and $\pm 12\%$ for lines with strengths roughly comparable to Hβ. The weakest lines reported for each nebula are subject to errors of about a factor of 2.

The spectra were absolutely calibrated so that we could derive the absolute surface brightnesses as viewed through the aperture of a given size; in the few instances in which the nebulae are smaller than the apertures, we could find total absolute fluxes. We present absolute Hβ surface brightnesses, $S(\mathrm{H}\beta)$, for almost all nebulae at the end of each column in units of 10^{-18} ergs cm^{-2} s^{-1} arcsec^{-1}. If a nebula is larger than the aperture, we divided the observed surface brightness by the angular area of the aperture (derived from Table 1); if it is smaller, by the angular area of the nebula (derived from the angular radius, ϕ, listed in Table 8). In a small number of cases we were unable to calibrate properly, or we present Hα surface brightnesses. *For all data, the reader should pay close attention to footnotes and to notes in the last column of Table 1.*

b) Central Stars

Many of the nebulae were centered in the observing aperture so that the nuclei could be detected, provided that they were bright enough. In several cases we noted a significant continuum that allowed (at least an approximate) determination of a magnitude. The observed continuum will actually be a mixture of nebular and stellar components. The former can be calculated from the observed Hβ surface brightness, the electron temperature, the ionic helium ratios, the interstellar extinction constant (see § III), and the theory provided by Brown and Mathews (1970); see Shaw and Kaler (1985, 1989) for details. Subtraction from the total then provides the stellar continuum, and the calibrations by Oke and Schild (1970) and Hayes (1970) yield the magnitudes.

We present the results in Table 7, where we give *B* and/or *V*-magnitudes for 17 stars. Each of these is accompanied to its right by a quantity called CS/TC, the ratio of the central star flux to that of the total continuum at the *B* and *V* wavelengths. These provide a crude index to the surety of the magnitude. The column labeled "Other" gives other measurements or determinations, with references keyed below. For purposes of comparison we calculate *B* from *V* or *V* from *B* with the extinctions listed in Table 8 and $(B-V)_0 = -0.4$ mag; these are indicated by parentheses. Included here are predictions of *V* calculated from the "crossover" method by Kaler and Jacoby (1989), indicated by square brackets. In this method, which is applied only to optically thick nebulae, they calcu-

TABLE 2

SPECTROPHOTOMETRY OF ABELL NEBULAE

λ	ID	A1	A2	A4	A5	A8	A9	A12	A15 CS[a]	A15 15"E	A18[b]	A19	A20 8"/N	A20 23"S	A20 25"W	A33 1	A33 2
3727	[O II]	...	83	74	250	...	...	...	...	...	343	...	...	...	...	194	82
3868	[Ne III]	...	124	66	...	...	...	...	...	...	54	...	...	...	...	151	73
3889	H,He I	...	17:	...	...	...	...	...	...	...	...	...	...	...	...	...	...
3967	[NeIII],H	...	47	22	...	...	...	...	...	...	...	...	...	...	...	...	...
4101	Hδ	...	15:	22	...	...	...	...	...	...	...	...	...	...	...	...	...
4340	Hγ	...	39	40	...	...	...	...	...	...	...	...	...	...	...	...	...
4363	[O III]	...	11:	9	...	...	...	...	...	...	...	...	...	...	...	...	...
4686	He II	< 55:	39	27	< 75	< 40	< 50	38	139	96	< 25	< 40	123	130	126	< 40	52
4861	Hβ	100:	100	100	100	100:	100	100	100	100	100	100	100	100	100	100	100
4959	[O III]	281	405	374	150:	428	394	365	88	86	174	260	161	174	...	507	391
5007	[O III]	1119	1319	1112	350	1102	1098	1190	167	276	487	863	491	622	...	1435	1140
5411	He II	...	...	...	...	...	...	3	...	...	...	...	...	...	...	...	...
5876	He I	...	...	8	...	...	...	15	...	...	...	...	...	...	...	...	...
6300	[O I]	...	...	...	...	...	...	24	...	...	...	...	...	...	...	...	...
6548	[N II]	...	...	...	1240	...	336	...	...	...	511	105	...	...	...	...	...
6563	Hα	1522	...	310	510	1180	815	505	397	308	838	285	437	388	...	405	356
6584	[N II]	966	...	66	3600	555	942	248	...	...	1673	375	...	...	...	203	63
6717	[S II]	167	...	15:	...	...	...	28	...	...	68:	...	...	...	...	...	...
6734	[S II]	157	...	10:	...	...	...	28	...	...	43:	...	...	...	...	...	...
10^{18}S(Hβ)		12.8	243	520	8.5	29	14.6	2650	255	431	33.4	32.9	70	127	69	35	42

λ	ID	A36	A54	A59	A62 CS	A62 25"W	A69	A70	A72	A75 3"W	A75 6"S	A80	A82	A84 A	A84 B
3727	[O II]	...	...	217	...	...	...	108	...	...	...	...	375[c]	315	747
3868	[Ne III]	20	...	...	...	...	...	81	...	...	...	...	...	95:	...
3889	H,He I	9	...	...	...	...	...	45:	...	...	...	...	...	...	...
3967	[NeIII],H	25	...	...	...	...	...	55:	...	...	...	...	...	...	...
4101	Hδ	24	...	...	...	...	...	...	...	...	...	...	...	44:	...
4340	Hγ	40	...	...	...	...	...	65:	...	...	...	...	...	...	...
4363	[O III]	...	...	...	...	...	...	8:	...	41	52	< 25	...	...	...
4686	He II	117	< 35	< 25	...	...	< 65	83	115	100	100	100	...	30	...
4861	Hβ	100	100	100	100	100	100:	100	100	375	353	93	100	100	100
4959	[O III]	115	240	177	133	492	229	350	548	1193	1191	293	298	241	44
5007	[O III]	335	799	613	382	768	730	1010	1522	...	...	...	881	740	834
5411	He II	...	...	...	...	...	...	...	...	...	...	...	...	...	...
5876	He I	...	...	...	...	...	...	...	...	...	...	29	...	...	...
6300	[O I]	...	83:	122	...	...	149	...	...	...	...	...	...	...	...
6548	[N II]	...	...	625	...	...	1810	38	...	650	771	588	131	...	...
6563	Hα	308	583	1188	...	...	1590	300	431	...	...	435	520	309	422
6584	[N II]	...	506	1831	...	...	6480	124	...	...	...	2011	419	453	1195
6717	[S II]	...	...	388	...	...	415	} 37	...	...	...	96	} 69	} 34	...
6734	[S II]	...	...	292	...	...	203					46			
10^{18}S(Hβ)		79	33	57	274	142	19.9	247	74	89	184	98	143	...	...

[a] Possible stellar absorption may distort intensities.
[b] Very poor agreement between [O III]/Hβ on red and blue exposures.
[c] Blue data scaled to [O III]; actually observed at a different position from [O III] and may be stronger than listed by a factor of 2 or more.

lated the V-magnitude required to make the hydrogen and ionized helium Zanstra temperatures equal to one another. Extensive comparison sets by Kaler and Jacoby (1989) and Jacoby and Kaler (1989) validate the method for stars that have not yet actually been observed.

The comparison of the new magnitudes with the other values is provided in Figure 1, where B and V are respectively plotted as filled and open symbols, and photoelectric, photographic, and crossover values as circles, squares, and triangles. There is good agreement for the brightest stars (NGC 3587 and NGC 6026), and an increasing disparity above magnitude 17. Between 17th and 20th magnitudes our determinations seem to be roughly half a magnitude too faint, whereas they may be too bright above $m = 21$. Nevertheless, they should be useful in the absence of other measurements.

Of all the nuclei detected, only one exhibits a possible emission line indicative of a wind, which is consistent with the generally low luminosities of these stars. The spectrum of the bright nucleus of Ba 1 displays a weak, narrow emission very close to the expected position of the O VI line at 5291 Å (Fig. 2), potentially adding one more object to the rare class of O VI stars (see Kaler and Shaw 1984). The star should be observed

TABLE 3

SPECTROPHOTOMETRY OF KOHOUTEK NEBULAE

λ	ID	K1-1	K1-3[a]	K1-7	K1-8	K1-9	K1-13[b]	K1-14[c]	K1-17	K1-20
3727	[O II]	...	...	231	...	...	206	...	...	121
3868	[Ne III]	...	...	74	...	...	112	...	...	35
3967	[Ne III],H7	...	...	37	...	...	...	...	...	...
4101	Hδ	...	...	31	...	...	...	...	...	...
4340	Hγ	...	...	47	...	...	...	...	...	41
4363	[O III]	...	...	8	...	...	...	...	...	...
4471	He I	...	...	5:	...	...	...	...	...	...
4686	He II	33	28	14	<35	≤35	<50	155	63	17:
4861	Hβ	100	100	100	100	100	100	100:	100	100
4959	[O III]	95	373	327	...	59	310	90	306	362
5007	[O III]	308	1316	997	<35	162	930	280	1025	1061
5200	[N I]	21	...	3:	...	22:	...	...	...	...
5876	He I	34	50	16	...	...	...	...	...	16:
6300	[O I]	29	...	18	...	...	...	...	...	...
6548	[N II]	468	...	...	...	1030	172	...	...	...
6563	Hα	354	2394	320	1468	444	373	280:	497	414
6583	[N II]	1510	82	232	373	3230	677	...	79	111:
6678	He I	...	...	9	...	...	...	...	...	...
6717	[S II]	50	...	37	...	} 107	...	...	...	} 58
6731	[S II]	24	...	24	...	...	...	...	...	...
10^{18}S(Hβ)		84	...	1190	34	53	16.3	...	81	91

λ	ID	K1-22	K3-27	K3-73	K3-74	K3-86	K3-91	K3-92
3727	[O II]	282	15?	288	144	141	167	162
3868	[Ne III]	47:	28:	88	73	72	41	59
3889	H, He I	13:	23	...	...	11	...	9
3967	[Ne III],H	39:	16	43	36	31	...	24
4101	Hδ	...	18	26	18	18	...	...
4340	Hγ	46	45	52	36	39	28	27
4363	[O III]	...	7:	12	...	15	...	4:
4471	He I	...	...	5.5:	...	...	...	...
4541	He II	...	3	...	...	...	...	...
4686	He II	<10	102	20	36	71	37	14
4711	[Ar IV]+HeI	...	14	...	...	...	...	...
4724	[Ne IV]	...	3:	...	...	...	...	...
4740	[Ar IV]	...	8	...	...	...	...	...
4861	Hβ	100	100	100	100	100	100	100
4959	[O III]	226	118	336	355	372	413	331
5007	[O III]	688	351	999	1064	1193	1290	1098
5411	He II	...	9	...	...	8	...	...
5754	[N II]	...	...	...	...	...	...	9
5876	He I	27:	...	11:	...	10	...	26
6300	[O I]	25:	8:	...	...	23	...	56
6363	[O I]	...	...	...	...	...	...	20
6542	[N II]	...	...	24[d]	82[e]	...	1210	...
6563	Hα	312	376	285[d]	539[e]	683	1370	809
6583	[N II]	79	...	90[d]	368[e]	200	3040	552
6717	[S II]	...	...	...	...	28	...	79
6731	[S II]	...	...	...	...	20	...	60
10^{18}S(Hβ)		36	1980	1127	179	348	162	845

[a] Both regions combined and averaged.
[b] Scaled to [O III].
[c] Confused by binary companion.
[d] Hα set to 285 on the basis of $c = 0$ from Hγ and Hδ; I[N II] scaled accordingly.
[e] Hα set to 539 on the basis of $c = 0.83$ from Hγ and Hδ; I[N II] scaled accordingly.

TABLE 4

SPECTROPHOTOMETRY OF MINKOWSKI NEBULAE AND A PEIMBERT-COSTERO OBJECT

λ	ID	M2-51	M2-53	M2-55 center	M2-55 lobes		M3-2	M3-3	M4-11	PC-21
3721	H 14,[S III]	...	...	...	...	...		1.7	...	
3726	[O II]	149	149	}166	}352	}262	}149	}229		}7
3729	[O II]	242	141							
3750	H 12	...	...	...	...	...	...	1.2	...	1:
3760	O III	...	...	...	...	...	...	0.6	...	3:
3770	H 11	...	3	...	...	...	...	1.5	...	1.2:
3797	H 10	...	4	...	...	...	...	3.3	...	2.9
3819	He I	...	...	...	...	...	...	1.2	...	0.2:
3835	H 9	...	6	...	...	...	...	5.6	...	4.2
3868	[Ne III]	64	73	61	57	68	157	87	...	34
3889	H 8, He I	18	15	15	10	13	22	17	...	7.4
3967	[Ne III]	26	27	30	30	36	50	36	...	18.3
3970	H 7	15	11	...	...	...	...	1.7	...	1.1
4026	He I, He II	...	3	...	...	...	...	0.8	...	3.3
4072	[S II]	7	3	...	...	...	...	...	...	...
4101	Hδ	16	21	21	...	...	12	21	...	19.4
4200	He II	...	...	...	...	...	...	0.7	...	1.2
4267	C II	...	...	...	...	...	...	≤ 0.4	...	1.4
4340	Hγ	43	45	...	33	34	37	39	...	36.6
4363	[O III]	7:	7	...	...	...	10	8.2	...	8.2
4471	He I	...	...	...	...	...	7	...	...	1.3
4541	He II	...	...	...	...	...	3	...	...	3.7
4571	Mg I	...	2:	...	...	...	...	...	...	...
4640	N III	...	...	...	...	...	...	1.3	...	6.0
4658	C IV	...	1:	...	...	...	...	...	...	...
4686	He II	20[a]	26	24	6:	13	83	29	66	103
4711+13	HeI,[ArIV]	...	2.5	...	...	...	8	2.7	...	8.6
4724	[Ne IV]	...	...	...	...	...	...	...	...	3.9:
4740	[Ar IV]	...	2.0	...	...	...	4	0.9	...	7.6
4861	Hβ	100	100	100	100	100	100	100	100	100
4921	He I	...	...	...	...	...	...	1.9	...	...
4959	[O III]	285	339	308	285	326	140	320	211	285
5007	[O III]	938	1118	947	874	1006	445	1030	697	913
5200	[N I]	10:	10	...	...	...	12	14.4	...	...
5411	He II	...	...	...	...	...	6	2.5	7	...
5754	[N II]	16	...	...	...	...	22	16.0	...	...
5876	He I	...	31	22	...	...	24	16.4	25	...
6300	[O I]	...	57	...	...	54	10	24.8	...	...
6312	[S III]	...	...	...	...	8	8	...	...	...
6363	[O I]	...	7	...	...	...	7	6.9	...	...
6548	[N II]	466	364	201	344	308	415	485	...	...
6563	Hα	626	785	794	688	722	419	436	500	...
6584	[N II]	1470	1113	696	1153	935	1290	1610	32	...
6678	He I	...	...	...	...	...	14	5.7	...	...
6717	[S II]	} ≤14	24	...	...	...	37	7.3	...	...
6731	[S II]		66	...	...	...	39	7.8	...	...
10^{18}S(Hβ)		471	760	220	110	110	1650	2590	≤1130	4150

[a] Blue observations confined to central star show *no* λ4686.

with good signal-to-noise ratio in the blue in order to look for O VI λλ3811 and 3834 in emission.

III. ANALYSIS OF THE OBSERVATIONS

a) Absolute Fluxes

Probably the most important fundamental datum regarding a planetary nebula is its absolute Hβ flux, which is conceptually akin to the magnitude of a star. Of the 75 nebulae considered here, only a little over half (42) have absolute fluxes available from standard wide-aperture interference-filter photometry. These are listed as log $F(\mathrm{H}\beta)_w$ in the second column of Table 8. They are taken from K83 (or from references cited therein), with the exceptions of K1-1 (from Perek 1971), NGC 6842 (O'Dell 1963), and M3-2, NGC 6026, and NGC 6072

TABLE 5

SPECTROPHOTOMETRY OF NGC NEBULAE

		NGC 246		NGC 650		NGC 1360		NGC 2438		NGC	NGC	NGC	NGC	NGC 6781		NGC	NGC 7094			NGC 7139			NGC 7293	
λ	ID	A	B	CS	25"W	A	B	CS	25"W	3587	4361	6026[a]	6072	A	B	6842	34"N	8"N	5"S	24"N	CS	25"W	Knot	100"E
3721	H14,[S III]	...	...	...	...	...	...	...	5	...	...	...	...	...	...	...	...	...	...	...	...	...	...	...
3726	[O II]	...	...	143	191	...	...	25	174	97	)<2	...	...	)236	)348	)12:	...	...	...	)206	143	225	...	...
3729	[O II]	...	...	194	267	...	...	26	217	127		...	...				...	...	...		164	288	...	...
3750	H 12	...	...	...	...	...	...	...	...	4	2:	...	...	...	...	...	...	...	...	...	...	...	...	...
3770	H 11	...	...	5:	...	...	...	...	...	3	3:	...	...	...	...	...	...	...	...	...	...	...	...	...
3797	H 10	...	...	5:	5	...	...	5:	...	5	4.5	...	...	...	...	...	...	...	...	...	...	...	...	...
3819	He I	...	...	...	...	...	...	...	...	2	...	...	...	...	...	...	...	...	...	...	...	...	...	...
3835	H 9	...	...	7	9	...	...	...	...	7	6.2	...	...	...	...	...	...	...	...	...	...	...	...	...
3868	[Ne III]	35	53	118	138	73:	81:	72	122	71	15	...	...	53	79	34	77	...	...	54	61	82	...	...
3889	H8,HeI	12	...	16	18	...	...	19	24	15	9	...	...	10	21	...	...	...	...	15	12	12:	...	...
3967	[Ne III]	)27	)41	)57	51	)54:	)40:	22	38	26	18	...	...	40	44	34	19	...	...	)25	)35	29	...	...
3970	H 7	...	...	...	12	...	...	18	18	16		...	...	...	...	...	...	...	...	...	...	12	...	...
4026	HeI, HeII	...	...	3:	...	...	...	4	2	...	1	...	...	...	...	...	...	...	...	...	...	...	...	...
4072	[S II]	...	...	5	3	...	...	5	3	...	1	...	...	...	...	...	...	...	...	...	...	...	...	...
4101	Hδ	28	29	33	32	...	...	33	32	24	23	...	...	26	20	33:	31	...	...	...	28	29	...	...
4200	He II	...	...	...	...	...	...	...	...	...	2	...	...	...	...	...	...	...	...	...	...	...	...	...
4340	Hγ	51	53	61	61	54	37:	61	61	44	43	...	...	39	31	38	44	...	...	50	53	49	...	...
4363	[O III]	9	16	14	11	9	17:	14	11	9	5.7	...	...	5:	10	11	13	...	...	<2	11	<6	...	...
4471	He I	...	...	2	7	...	...	2:	7:	...	...	...	...	...	...	...	...	...	...	...	...	5:	...	...
4541	He II	4	6	3	4	...	...	3:	...	...	3.1	...	...	...	...	...	11	...	...	...	...	...	...	...
4634	N III	...	...	...	...	...	...	...	...	...	0.4	...	...	...	...	...	...	...	...	...	...	...	...	...
4640	N III	...	...	...	...	...	...	...	...	...	0.4	...	...	...	...	...	...	...	...	...	...	...	...	...
4658	C IV	...	...	...	...	...	...	...	...	...	1.8	...	...	...	...	...	...	...	...	...	...	...	...	...
4686	He II	119	105	72	66	86	58	95	21	23	107	85	48	≤3	6:	42	122	134	138	<3	25	<8	36	31
4712	HeI,[ArIV]	10	14	6:	...	16	...	10	1:	...	8.7	...	...	...	...	...	13	...	...	...	...	...	...	...
4724	[Ne IV]	...	...	...	...	...	...	...	...	...	1.6	...	...	...	...	...	...	...	...	...	...	...	...	...
4740	[Ar IV]	7	11	3:	3:	19	...	9	...	...	5.4	...	...	...	...	...	9	...	...	...	...	...	...	...
4861	Hβ	100	100	100	100	100	100	100	100	100	100	100	100	100	100	100	100	100	100	100	100	100	100	100
4959	[O III]	136	215	...	...	212	220	...	...	...	64	320	456	317	286	294	181	194	157	203	...	...	317	341
5007	[O III]	410	638	...	...	658	610	...	...	...	199	980	1519	998	879	951	557	694	667	594	...	...	982	1061
5200	[N I]	...	...	...	...	...	...	...	...	...	...	...	7:	10	10	...	...	...	...	15	...	...	...	...
5411	He II	10	8	...	...	21	...	...	...	...	7.6[b]	...	7	...	...	...	...	...	...	...	...	...	...	...
5754	[N II]	...	...	...	...	...	...	...	...	...	...	...	12	8	13	...	...	...	...	...	...	...	...	...
5876	He I	...	...	...	...	...	...	...	...	...	...	...	24	23	31	23	...	...	...	25	...	...	...	...
6300	[O I]	...	...	...	...	...	...	...	...	...	...	...	47	39	77	...	...	...	...	86	...	...	≤26	<23
6363	[O I]	...	...	...	...	...	...	...	...	...	...	...	17	9	28	...	...	...	...	29	...	...	...	...
6435	[Ar V]	...	...	...	...	...	...	...	...	...	2.1	...	...	...	...	...	...	...	...	...	...	...	...	...
6548	[N II]	...	...	...	...	...	...	...	...	...	...	...	212	294	326	...	...	...	...	253	...	...	51	53
6563	Hα	316	308	...	...	279	222:	...	...	...	294	580	521	645	601	662	336	478	294:	510	...	...	333	381
6584	[N II]	...	...	...	...	...	...	...	...	...	<1.6	...	719	949	1055	34	...	...	...	743	...	...	153	160
6678	He I	...	...	...	...	...	...	...	...	...														
6717	[S II]	...	...	...	...	...	...	...	...	...	...	...	10:	64	54	...	...	...	...	)239	...	...	...	...
6731	[S II]	...	...	...	...	...	...	...	...	...	...	...	13:	52	53	...	...	...	...	...	...	...	...	...
10^{18}S(Hβ)		1040	598	3060	2510	...	...	1380	2390	1510	7780	509	1730	1640	1440	770	202	191	100	476	457	383	423	424

[a] Approximate: absorption-line nucleus.

TABLE 6

SPECTROPHOTOMETRY OF A MISCELLANY OF NEBULAE

λ	ID	Ba 1 CS	Ba 1 W	DHW 1[a]	He1-6	IC 5148	Jn 1 A	Jn 1 B	Lo 4	LoTr 5[a]	Pu 1	PW 1
3726	[O II]	...	...	...	...	...	...	...	...	...	}429	...
3729	[O II]	...	...	...	...	...	...	...	...	...		...
3868	[Ne III]	30:	...	...	...	...	120	...	35	...	48	...
3967	[Ne III],H7	...	...	...	...	...	...	...	...	...	38:	...
4101	Hδ	...	...	...	...	...	...	...	20:	...	...	...
4340	Hγ	28:	...	...	...	...	...	...	41	...	...	...
4363	[O III]	...	...	...	...	...	...	...	11	...	...	...
4686	He II	102	88	...	17	45	76	83	93	...	<18	<33
4711	[Ar IV]	...	...	...	...	...	...	...	15	...	...	...
4740	[Ar IV]	...	...	...	...	...	...	...	17	...	...	...
4861	Hβ	100	100	...	100	100	100	100	100	...	100	100
4959	[O III]	159	204	...	272	197	459	522	131	244	128	45:
5007	[O III]	487	615	254	896	630	1412	1419	357	723	441	369
5200	[N I]	...	...	...	7	...	...	...	...	...	...	...
5754	[N II]	...	...	...	9	...	...	...	...	...	...	...
5876	He I	...	...	...	24	15	...	...	...	...	...	...
6300	[O I]	...	...	...	42	...	...	...	...	...	...	...
6548	[N II]	...	...	...	222	32[b]	...	...	...	...	246	...
6563	Hα	487	460	285	590	501[b]	365	334	277	285	662	340:
6584	[N II]	...	...	...	738	65[b]	162	167	...	...	873	280:
6717	[S II]	...	...	...	63	...	...	}102	...	...	...	...
6734	[S II]	...	...	...	45	...	...		...	...	...	...
10^{18}S(Hβ)		78	67	54[c]	830	254	146	106	113	29[c]	45	9.5

λ	ID	Sh1-89	VV1-2	VV1-4	We 1	We 2	We 3[d]	We 5
3726	[O II]	}132:	...	65	}32	}257	...	...
3729	[O II]		...	45			...	...
4340	Hγ	...	...	31	...	...	...	41
4686	He II	39	<16	<10	15:	<100	...	95
4861	Hβ	100	100	100	100	100:	...	100
4959	[O III]	175	...	...	379	147	...	81
5007	[O III]	737	...	...	1117	355	442	259
5200	[N I]	12	...	...	...	...	...	...
5411	He II	5	...	...	...	...	...	...
5876	He I	31	...	...	...	...	...	...
6300	[O I]	49	38:	...	...	...	...	...
6363	[O I]	20	...	...	...	...	...	...
6548	[N II]	394	...	81	...	...	...	...
6563	Hα	551	902	790[e]	...	916	553	606
6584	[N II]	1271	281	306	...	1768	1220	...
6717	[S II]	79	47	54	...	...	...	...
6734	[S II]	62	44	60	...	...	...	...
10^{18}S(Hβ)		42	55	500	6.6	6.6	32[c]	228

[a] Scaled to $I(\mathrm{H}\alpha) = 285$.
[b] $I(\mathrm{H}\alpha)$ and I[N II] are very uncertain; relative I[N II]/I[Hα] is accurate.
[c] Hα surface brightness.
[d] Hβ not observed; $I(\mathrm{H}\alpha)$ set at 820 on the basis of extinction (see Table 8).
[e] Saturated: may be higher.

TABLE 7

CENTRAL STAR MAGNITUDES

NEBULA	B (mag)	$(CS/TC)_B$	V (mag)	$(CS/TC)_V$	OTHER B (mag)	OTHER V (mag)	REFERENCE
Ba 1	18.7	0.98	...	...	17.6	...	1
K1-9	...	...	19.5	0.96	19.1	(19.1)[a]	1
K3-73	20.8	0.56	...	...	(20.8)	[21.18][b]	2
K3-86	20.9	0.56	21.6	0.18	(23.2)	22.75	3
K3-91	...	...	19.6	0.93	...	>20.50[c]	3
K3-92	...	...	20.6	0.40	...	[23.31]	2
Lo 4[a]	22.0	0.47	20.5	0.74	...	...	
M2-51	19.2	0.98	20.4	0.55	(19.8)	[19.52]	2
M2-53	21.2	0.59	...	...	(22.8)	[22.27]	2
M2-55	21.2	0.74	21.1	0.50	(19.7)	[19.18]	2
M4-11	...	...	18.7	0.60	17.9	18.0	4
NGC 2438	18.3	0.89	...	...	(17.6)	17.88	5
NGC 3587	15.4	0.99	...	...	15.59	...	6
NGC 6026	13.5	1.0	13.5	1.0	13.35	13.29	7
NGC 7139	19.9	0.91	...	...	(18.84)	18.72	3
VV 1-4	19.5	0.95	18.9	0.90	11.9	...	1
We 5	19.7	0.87	19.1	0.82	18.9	(18.6)	8

[a] Values in parentheses calculated from measured (or predicted) B or V and extinction.

[b] Crossover (predicted) magnitude placed in brackets.

[c] Kaler and Jacoby 1989 predict $V = 26.7$ mag.

REFERENCES.—(1) Kohoutek, in Perek and Kohoutek 1967, with 0.5 added; (2) Kaler and Jacoby 1989; (3) Jacoby and Kaler 1989; (4) Kwitter, Jacoby, and Lydon 1988; (5) Kaler and Feibelman 1985, corrected according to new extinctions; (6) Shao and Liller 1973; (7) Shaw and Kaler 1989; (8) Weinberger 1977.

(Shaw and Kaler 1989). In addition, an uncertain absolute flux for K1-3 (Abell 38) was derived from Abell's (1966) Hα photographic brightness as given in Cahn and Kaler (1971), and our extinction and [N II]/Hα flux ratio.

For 10 other nebulae, the absolute Hβ flux can be derived from the absolute radio flux densities listed in Table 9. We use the relation derived by Oster (1961) as expressed in Cahn and Kaler (1971), the [O III] electron temperatures, He^+/H^+, and He^{+2}/H^+ ratios given in Table 10 below, and the extinctions in column (5) of Table 8 (see § III*b* below). In cases in which no He^+/H ratios are available, we set it equal to $0.1 - He^{+2}/H^+$. If I(He II λ4686) is an upper limit, we adopted He^{2+}/H^+ appropriate to one-half of the limit. The results are shown in parentheses in the second column of Table 8. They will certainly not be as accurate as they are for the directly observed Hβ fluxes. The radio flux densities are typically accurate to ±0.10 in the log (however, note the high error for A18); errors in the temperatures and He/H ratios possibly add ±0.04 and ±0.02, respectively, and uncertainties in extinction perhaps another ±0.10. Compounding quadratically, we see that the calculated Hβ fluxes are good to about ±0.15 in the log, still quite acceptable. For an additional seven objects, we derived F(Hβ) from

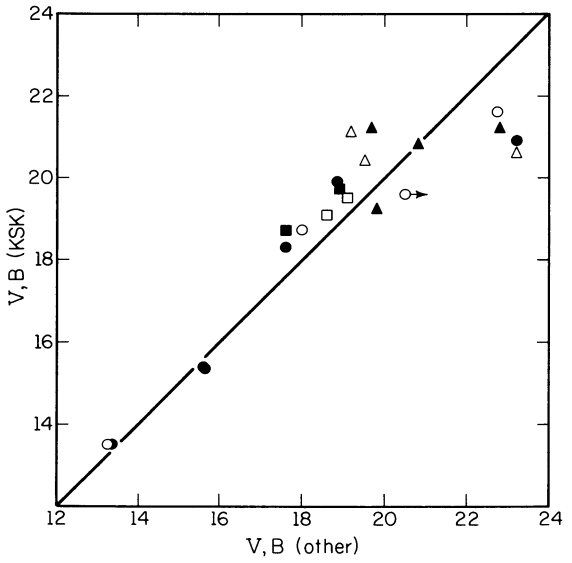

FIG. 1.—New magnitudes of Table 7 plotted against other determinations. Filled symbols represent B-magnitudes, and open symbols V-magnitudes. Circles, squares, and triangles respectively represent other determinations as found photoelectrically, photographically, and by the predictive crossover method (see text).

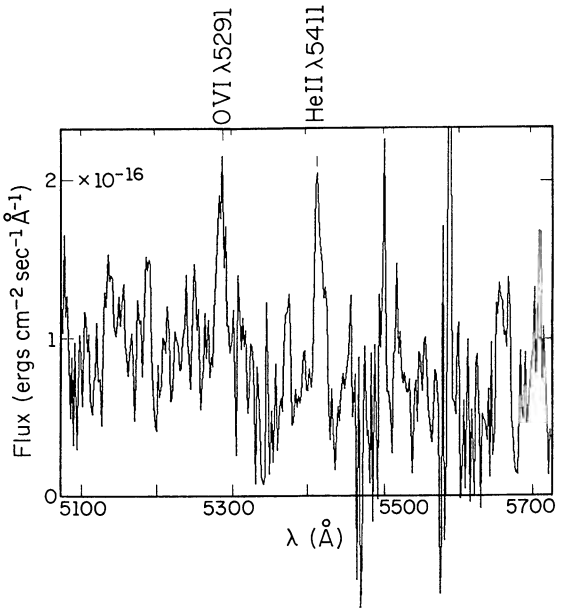

FIG. 2.—Spectrum of the nucleus of Ba 1. Nebular He II λ5411 and stellar O VI λ5291 are indicated.

TABLE 8

NEBULAR PARAMETERS

Nebula	$-\log F(H\beta)_w$	Ø"	$-\log F(H\beta)_s$	c	D(pc)	R(pc)
A 1	...	23.5	13.65	2.19	2230	0.26
A 2	12.37	15.5	12.74	0.59[a]	3500	0.26
A 4	12.49	10	11.83	0.11	5700	0.28
A 5	12.9	64	13.0	0.76	1680	0.52
A 8	13.0	30	13.1	1.86	1670	0.24
A 9	[13.92][b]	18.5	13.8	1.37	4260	0.38
A 12	(11.73)[b]	18.5	11.54	0.75	2020	0.18
A 15	12.47	17	12.51	0.10	4130	0.34
A 18	[(12.99)]	37	12.84	1.41	1800	0.32
A 19	...	33.5	12.94	0.00	≤3570	≤0.58
A 20	12.04	34	12.49	0.48	1880	0.31
A 33	11.3	134	11.66	0.38	610	0.40
A 36	10.86	196	11.0	0.10	450	0.43
A 54	...	28	13.09	0.94	2770	0.38
A 59	[(13.07)]	43	12.48	1.87	1380	0.29
A 62	12.01	81	11.37	2.18[c]	500	0.20
A 69	...	11	14.12	2.25	≤4260	≤0.23
A 70	12.34	21	12.47	0.07	3480	0.35
A 72	11.88	64	12.02	0.54	1160	0.36
A 75	12.00	29	12.44	1.18	1460	0.21
A 80	11.80	70	11.82	0.55	≤1050	≤0.36
A 82	11.72	47	12.00	0.79	≤1160	≤0.26
A 84	11.74	66	...	0.33	1180	0.38
Ba-1	12.44	20	12.77	0.66	2850	0.28
DHW 1	...	64	12.6:[d]	...	≤2070	≤0.64
Hel 6	...	11.2	12.19[e]	0.95	≤3150	≤0.17
		16.8			≤2470	≤0.20
IC 5148	...	60	11.5:[f]	0.4[f]	<1080	<0.31
Jn-1	11.48	166	10.96	0.27	620	0.50
K1-1	12.36	21.7	12.90	0.28	≤3120	≤0.33
K1-3	12.28:[g]	46	...	2.78	610	0.14
		62			510	0.15
K1-7	12.13	17	11.97	0.15	≤3450	≤0.28
K1-8	(12.88)	39.5	12.77	2.14	1140	0.22
K1-9	...	21.5	12.95[e]	0.58	3590	0.37
		30			2940	0.43
K1-13	(11.07)	83	12.45	0.35	≤ 730	0.29
K1-14	12.40	24	...	0.00	3400	0.40
K1-17	...	22.5	12.89	0.73	3170	0.35
K1-20	12.93	17	13.08	0.49	4260	0.35
K1-22	11.42	91	11.45	0.12	≤ 920	≤0.41
K3-27	12.11	8.2	12.38[h]	0.36	4800	0.19
K3-73	...	8	12.64	0.0	7350	0.29
K3-74	...	10	13.36	0.83	≤6110	≤0.30
K3-86	...	4.7	13.62	1.14	9390	0.21
K3-91	(14.41)	2.9	14.54[h]	2.06	≤11400	≤0.16
K3-92	(13.57)	3.65	13.50[h]	1.37	9350	0.17
Lo 4	...	24	12.69	0.00	3890	0.45
LoTr 5	11.8	263	11.7[i]	0.00	610	0.78
M2-51	11.97	21	11.91[e]	1.03	≤1880	≤0.19
		35			≤1390	≤0.24
M2-53	(12.82)	7.5	12.87:	1.33	4340	0.16
M2-55	12.16	25	12.55	1.24	≤1670	≤0.20
M3-2	12.61	4	13.04[h]	0.50	8700	0.17
M3-3	12.29	6.4	12.48	0.56	5530	0.17
M4-11	[12.01]	10.6	12.40	0.74	3300	0.17
NGC 246	10.53	125	10.40	0.12	510	0.31
NGC 650	10.68	36	10.58[e]	0.20[c]	≤1100	≤0.19
		69			≤ 750	≤0.25
NGC 1360	10.2	198	...	0.00	350	0.33
NGC 2438	11.04	35	10.79[e]	0.20[c]	1320	0.22
		65			910	0.29
NGC 3587	10.42	100	10.33	0.01[c]	≤ 580	≤0.28
NGC 4361	10.53	58	10.09	0.04	830	0.23
NGC 6026	11.65	23	12.07	0.93	1610	0.18
NGC 6072	11.22	21	11.62	0.79	≤1490	≤0.15
NGC 6781	11.21	55	10.69[e]	1.02	750	0.20
		74			630	0.23

TABLE 8—*Continued*

Nebula	$-\log F(H\beta)_w$	ϕ"	$-\log F(H\beta)_s$	c	D(pc)	R(pc)
NGC 6842	11.73	29	11.69	1.10	1340	0.19
NGC 7094	11.77	47	11.74	0.34	1460	0.33
NGC 7139	11.80	39	11.68	0.76	1360	0.26
NGC 7293	9.37	402	9.67[j]	0.04[c]	≤ 150	≤0.30
PC 21	...	6.7	11.90[e]	0.73[k]	4150	0.14
		12.0			2930	0.17
Pu 1	[13.20]	33	12.81	1.10	2450	0.39
PW 1	10.85	600	10.97	0.23	220	0.63
Sh1-89	...	19	11.78[e]	0.86	1980	0.18
		84			810	0.33
VV1-2	(11.65)	125	11.57	1.51	440	0.27
VV1-4	(11.07)	65	11.18	1.35[l]	540	0.17
We 1	...	10	14.69	0[f]	<16500	<0.80
We 2	[13.39]	46	13.36	1.53	1800	0.40
We 3	[13.18]	58	13.2[i]	0.86[m]	1930	0.54
We 5	(13.32)	7.5	13.40	0.99	6470	0.24

[a] From $H\gamma/H\beta$; average of this value and that from K83 yields $c = 0.48$, which is used in subsequent analysis.

[b] Values in parentheses derived from radio fluxes of Table 8, electron temperatures of Table 10, and the extinctions of the fifth column; values in brackets derived from Kwitter and Jacoby's 1989 Hα fluxes and the extinctions of the fifth column; the fluxes for A18 and A59 are weighted means of converted radio and Hα fluxes weighted 1:5 and 9:1, respectively.

[c] From Kaler 1983.

[d] From Hα assuming $c = 0$; D and R are upper limits.

[e] Average of fluxes computed on the basis of inner and outer radii.

[f] Flux is lower limit; occulted by dome; c is average of values from Hα and from KF.

[g] Converted from Abell's F_{red}.

[h] Total flux (object smaller than aperture).

[i] From Hα and c.

[j] In hole.

[k] From $H\gamma/H\beta$ and $H\delta/H\beta$.

[l] Lower limit; D and R are upper limits.

[m] From central star color from Kwitter, Jacoby, and Lydon 1988.

the Hα fluxes presented by Kwitter and Jacoby (1989) and our extinctions. These are noted by square brackets in Table 8. The fluxes presented for A18 and A59 are averages of those found from the radio and Hα.

For all but three of our nebulae, we derived absolute total Hβ fluxes from the surface brightnesses of Tables 2–6 and the angular radii (ϕ) given in Table 8, where the latter were taken from Perek and Kohoutek (1967) or the discovery papers (see the notes to Table 1). In the instances in which there are two radii (inner and outer for double-shell objects) we give the average of the values that use each radius. The results, presented in the fourth column, are called log $F(H\beta)_s$, and are plotted against log $F(H\beta)_w$ (including those derived from the radio and Hα fluxes) in Figure 3. For the four double-shell nebulae, log $F(H\beta)_s$ calculated with the inner and outer radii are shown by connected open and filled circles, respectively, with the average (the value in the table) indicated by a horizontal bar. There is quite a large scatter, as expected, since the surface brightnesses of the nebulae are hardly uniform, and we sample but one or two points. Yet the correlation is very strong, which shows that our measurements are usable for certain purposes as long as the errors are kept in mind. Two-thirds of the points fall within ±0.3 of the 1:1 line, and nearly all within ±0.4, which we adopt as the extreme error for log $F(H\beta)_s$. Note that the fluxes of DWH 1 and LoTr 5 were derived from the Hα surface brightness and the extinction constants (§ III*b*), and are even more uncertain.

TABLE 9

RADIO FLUX DENSITIES

Nebula	ν (mHz)	$F_\nu d\nu$ (Jy)	Reference
A12	5	0.036	1
	5	0.036	2
A18	14.7	0.015[a]	3
A59	5	0.018	1
K1-8	5	0.053	1
	5	0.066	2
K1-13	14.7	0.052	3
K3-91	5	0.0015	1
K3-92	5	0.002	1
M2-53	5	0.011	1
VV 1-2	1.5	0.300	1
VV 1-4	1.5	0.327	1
	14.7	0.498	3

[a] High error, perhaps ±65%.

REFERENCES.—(1) Zylstra, Pottasch, and Bignell 1989; (2) Milne 1979; (3) Milne and Aller 1982.

b) Interstellar Extinction

Before we can proceed with any analysis, we must determine the degree of interstellar reddening. We found the extinction constants, c (the logarithmic extinctions at Hβ), from the Hα/Hβ intensity ratios [$I(H\alpha)$ in Tables 2–6], the theoretical value of 285 (Brocklehurst 1971), and f_λ (Whitford 1958) = −0.332; see Seaton (1960) for the formulation of the standard reddening curve. The results are placed in the fifth

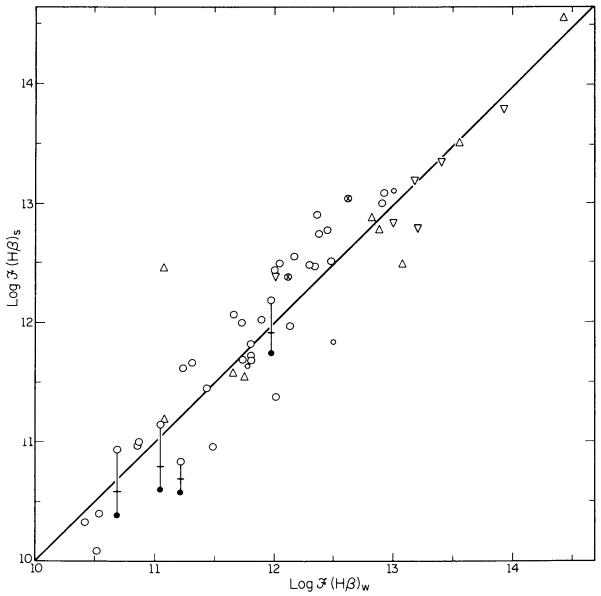

FIG. 3.—The log of our Hβ fluxes, log $F(H\beta)_s$, derived from surface brightnesses, plotted against log $F(H\beta)_w$, derived from total photometry. *Circles*: wide-aperture Hβ photometry; *triangles*: Hβ fluxes converted from radio fluxes; *inverted triangles*: Hβ fluxes converted from Hα fluxes or Hβ fluxes converted from both Hα and radio fluxes. Four double-shell nebulae are represented by lines that connect open and closed circles that denote log $F(H\beta)_s$ calculated by adopting the inner and outer radii, respectively; the horizontal crossbar represents the average, which should be closer to the truth.

column of Table 8. There are a few exceptions. The extinction for A2 is derived from our Hγ and Hδ values averaged with that from K83. The Hα intensity of IC 5148 is quite uncertain, and we average our result with that from Kaler and Feibelman (1985). Check the footnotes for others. From seven nebulae for which we have more than one set of data, we estimate the errors in c to be about ± 0.10. The extinctions derived here are compared with those from K83 in Figure 4. The points follow the 45° line, but there is considerable scatter that can likely be

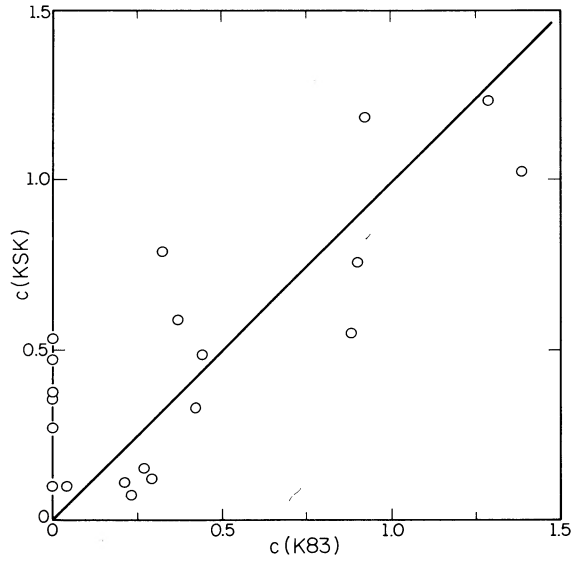

FIG. 4.—Extinctions from this paper, c(KSK), plotted against those from Kaler (1983), c(K83). The solid line shows the 1:1 relation.

related to the filter photometry, implying errors in the K83 extinctions of the order of ± 0.2.

c) *Distances and Radii*

We calculate nebular distances and radii from the Cahn and Kaler (1971) formulation of the Shklovsky method, under which we assume that all nebulae have the same mass and are optically thin. These assumptions are certainly not entirely correct, and there will be significant individual errors, but there is no obviously better alternative; they should at least provide us with statistically useful values. The computed distances (D) and radii (R), both in parsecs, are placed in the last two columns of Table 8, where we use the data of the second through fifth columns, and preferentially adopt log $F(H\beta)_w$. D and R are calculated twice for double-shell objects with two radii; for general consistency, we prefer the smaller, since the outer shells of many objects may not be detected. However, our criterion for inclusion in this study is that the radius based on the outer value of ϕ be greater than 0.15 in order to include all possible objects, i.e., we prefer to include a few that possibly do not belong in the set rather than to exclude any.

Some nebulae are almost certainly optically thick, so that D and R will be upper limits. Our criteria for thickness are (1) equality (or at least similarity, within 10%) in the H and He II Zanstra temperatures; and (2) strong [O II] or [N II] in the cases in which true Zanstra temperatures cannot be computed because the central star magnitude has not been determined. Examples are A80, K1-22, and NGC 3587 for the first case, and A82, K3-74, and K3-91 for the second. We discuss the matter further below in § III*e*.

d) *Chemical Compositions*

We use the Illinois abundance code ABUNDR to derive electron temperatures, densities, and chemical compositions, after correcting all the data for interstellar reddening according to the extinctions in Table 8 and the Whitford (1958) reddening curve. The code produces exact three- and five-level calculations (as appropriate) with the latest available atomic parameters; see Kaler (1985*a*) for details. The [O III] and [N II] electron temperatures are listed in the second and third columns of Table 10. These large nebulae are so faint that there are few actual measurements of temperature: in only 19 cases could we detect either [O III] λ4363 or [N II] λ5754. In all other instances we adopt the temperatures in accord with the He II λ4686 strength and the correlations given by Kaler (1986); these are placed in parentheses.

For about the same number of nebulae we were able to detect the [S II] λ6723 doublet, or used dispersions high enough to resolve the [O II] λ3727 pair, and were able to derive densities. These are placed in the next two columns of Table 10. In the other cases we simply calculated rms densities from the distances and radii and an assumed filling factor of 0.65; these are placed in parentheses in the N_e[S II] column. They are primarily informational, since these low values have little effect on, or importance in, the abundance calculations.

We list the ionic oxygen abundances (O^+/H^+ and O^{+2}/H^+) in the next two columns, which respectively incorporate T_e[N II] and T_e[O III]. Since some of the nebulae were not observed in the blue, we do not always have the [O II] λ3727 intensity from which to derive O^+/H^+, and had to make use of estimates based on the strengths of [S II] λ6723 and [O I] λ6300, which correlate linearly with that of [O II] (Kaler 1985*a*). Calculations based on these correlations are built into

the abundance code. The resulting abundance ratios are set into square brackets or parentheses denoting respectively whether [S II] or [O I] was used; the estimate from [O I] is preferred. The errors to be applied to these estimates are likely to be high. The ionic helium abundances are shown in the next pair of columns. He^+/H^+ was derived from T_e[O III] and one or more of He I $\lambda\lambda$4471, 5876, and 6678 where, in the few cases in which it was necessary, we used the collision-correction equation given by Clegg (1987). He^{+2}/H^+ is found from He II λ4686. Finally, N^+/H^+ is presented in the tenth column, where of course we use T_e[N II]. The Hβ effective recombination coefficient is calculated with T_e[O III], which may produce a systematic error in the abundances if much of the nebular gas is in a lower ionization state and if the two temperatures are significantly different, which in general they are not. An extreme case is M3-2, for which T_e[O III] is well above T_e[N II], but for which the O^+ abundance is about that of O^{+2}. If we use a mean temperature, the oxygen abundance will drop by 30%, still not a very significant amount. The problem is hereafter ignored.

In the next three columns we give total abundance ratios: O/H, where we correct for higher ionization stages by multiplying $(O^+ + O^{+2})/H^+$ by $(1 + He^{+2}/H^+)$ in accord with Seaton (1968); He/H, where we simply sum the ionic values;

TABLE 10

ELECTRON TEMPERATURES, DENSITIES, AND ABUNDANCES

	T_e [O III]	T_e [N II]	N_e [S II]	N_e [O II]	10^4 O^+/H	10^4 O^{+2}/H^+	He^+/H^+	He^{+2}/H^+	10^4 N^+/H^+	10^4 O/H	He/H	N/O	Ne^{2+}/O
A 1	(10300)	(10200)	420	...	[1.06]	3.06	...	...	0.33	≥4.1	...	[0.31]	...
A 2	11700	(10200)	(100)	...	0.37	2.89	...	0.036	...	(4.9)	...	...	0.19
A 4	11400	(10200)	(90)	...	0.26	2.80	0.082	0.024	0.10	4.0	0.106±0.02	0.40	0.10
A 5	(10300)	(10200)	(15)	...	1.43	1.21	...	...	3.68	>2.6	...	2.57	...
A 8	(10300)	(10200)	(130)	...	...	3.43	...	...	0.24	>3.4	...	...	...
A 9	(10300)	(10200)	(40)	...	...	3.45	...	...	0.62	>3.5	...	...	...
A 12	(12100)	(10200)	560	...	(0.80)	2.38	0.076	0.036	0.23	4.7	0.113	(0.29)	...
A 15[a]	(15300)	(10200)	(50)	...	...	0.32	...	0.091	...	...	≥0.091	...	...
A 18	(10300)	(10200)	(70)	...	3.11	1.53	...	...	1.01	4.6	...	0.33	0.25
A 19	(10300)	(10200)	(10)	...	...	2.85	...	...	0.65	>2.9	...	...	...
A 20[b]	(17500)	(10200)	(65)	...	...	0.54	...	0.130	...	...	≥0.130	...	...
A 33[c]	(12800)	(10200)	(30)	...	0.31	2.05	...	0.048	0.078	(4.2)	...	0.25	0.09
A 36	(16600)	(10200)	(25)	...	...	0.34	...	0.114	...	...	>0.114	...	...
A 54	(10300)	(10200)	(35)	...	(2.41)	2.47	...	...	0.45	>4.9	...	(0.19)	...
A 59	(10300)	(10200)	(175)	...	2.74	1.77	...	...	0.80	>4.5	...	0.29	...
A 62[d]	(10300)	(10200)	(240)	...	...	2.0	...	...	...	>2.0	...	0.01?[d]	...
A 69	(10300)	(10200)	(160)	...	(1.85)	2.09	...	...	2.02	>3.9	...	(1.1)	...
A 70	9700	(10200)	(40)	...	0.43	4.42	...	0.072	0.23	...	...	0.54	...
A 72	(16800)	(10200)	(40)	...	...	1.48	...	0.118	...	...	≥0.118	...	...
A 75[d]	(12800)	(10200)	(90)	...	...	2.02	...	0.047	...	(>3.6)	...	<0.10[d]	...
A 80	(10600)	(10200)	(40)	...	(2.85)	0.94	...	...	2.32	>3.8	...	(0.82)	...
A 82	(10300)	(10200)	(120)	...	2.19	2.60	...	...	0.41	>4.8	...	0.18	...
A 84A	(11500)	(10200)	(35)	...	1.25	1.77	...	0.027	0.71	(4.0)	...	0.57	0.18
B	(10300)	(10200)	(35)	...	3.20	2.18	...	...	1.47	5.38	...	0.46	...
Ba 1CS	(15600)	(10200)	(90)	...	...	0.50	...	0.105	...	...	≥0.105	...	...
DHW 1	(10300)	(10200)	(10)	...	...	2.50	...	...	...	>2.5	...	...	...
Hel-6	(10800)	(10300)	(370)	...	(1.24)	2.43	0.111	0.016	0.61	4.2	0.127	(0.49)	...
IC 5148	(12400)	(10200)	(60)	...	...	1.21	0.096	0.042	0.065	>1.2	0.138	...	...
Jn 1A	(14200)	(10200)	(15)	...	[1.09]	1.96	...	0.072	0.18	[(8.95)]	...	[0.17]	0.05
Kl-1	(11700)	(10200)	(50)	...	(1.22)	0.70	0.23	0.03	2.00	2.2	0.26	(1.6)	...
Kl-3	(11900)	(10200)	(760)	...	...	2.37	0.092	0.033	0.016	3.2	0.125	...	...
Kl-7	10800	(10200)	(80)	...	0.86	2.91	0.112	0.012	0.37	4.2	0.124	0.43	0.15
Kl-8	(10300)	(10200)	(190)	...	[0.82]	...	...	...	0.13	0.8	...	[0.16]	...
Kl-9	(10300)	(10200)	(35)	...	[1.82]	0.54	...	...	3.72	2.4	...	[2.1]	...
Kl-13	(10300)	(10200)	(10)	...	0.82	3.07	...	...	0.89	3.9	...	1.1	0.30
Kl-14	(18700)	(10200)	(30)	...	...	0.22	...	0.154	...	...	>0.15[e]	...	...
Kl-17	(13600)	(10200)	(45)	...	[0.53]	1.50	...	0.062	0.067	2.6	...	[0.13]	...
Kl-20	(10700)	(10200)	(40)	...	0.56	3.10	0.095	0.015	0.14	4.3	0.110	0.24	0.09
Kl-22	(10300)	(10200)	(30)	...	1.04	2.30	0.189[f]	...	0.13	3.3	0.189[f]	0.13	0.14
K3-27	(15700)	(10200)	(270)	...	0.05	0.39	...	0.101	...	...	≥0.10	...	...
K3-73	11900	(10200)	(80)	...	0.89	2.22	0.084	0.018	0.14	3.8	0.102	0.16	0.13
K3-74	(12000)	(10200)	(85)	...	0.79	2.21	...	0.035	0.29	(4.4)	...	0.37	0.14
K3-86	15100	(10200)	(190)	...	0.81	1.35	0.045	0.074	0.11	5.8	0.119	0.14	0.06
K3-91	(10300)	(10200)	(335)	...	2.49	3.77	...	...	1.20	6.3	...	0.48	0.20
K3-92	9900	12300	113	...	0.85	3.83	0.098	0.014	0.28	5.3	0.111±0.011	0.33	0.27

TABLE 10—*Continued*

	T_e [O III]	T_e [N II]	N_e [S II]	N_e [O II]	10^4 O^+/H	10^4 O^{+2}/H^+	He^+/H^+	He^{+2}/H^+	N^+/H^+	10^4 O/H	He/H	N/O	Ne^{2+}/O
Lo 4	20500	(10200)	(20)	...	...	0.24	...	0.090	...	...	≥0.09	...	...
LoTr 5	(10300)	(10200)	(5)	...	...	2.45	...	...	...	...	...	...	...
M2-51	11000	9900	(250)	...	2.97	2.37	...	...	0.84	5.3	...	0.41	0.16
M2-53	10400	(10200)	10^5:	600[g]	2.75	3.37	0.118	0.026	0.74	7.5	0.143	0.27	0.20
M2-55-C	(11300)	(10200)	(130)	...	1.27	2.25	0.090	0.024	0.41	4.4	0.114	0.32	0.19
L1	(10300)	(10200)	(130)	...	2.88	2.72	...	0.006	0.85	5.9	...	0.29	0.19
L2	(10600)	(10200)	(130)	...	2.11	2.90	...	0.013	0.66	5.7	...	0.31	0.21
M3-2	18700	(11000)	720	...	0.39	0.33	0.135	0.084	0.86	1.2	0.219±0.013	2.0	0.26
M3-3	11600	9000	700	...	1.86	2.36	0.094	0.027	2.18	5.4	0.120±0.005	1.2	0.13
M4-11	(13800)	(10200)	(220)	...	...	0.99	0.135	0.065	0.03	1.5	0.20	...	...
NGC 246A	15400	...	(65)	...	...	0.49	...	0.115	...	...	≥0.115	...	...
B	16100	...	(65)	...	...	0.68	...	0.102	...	...	...	...	...
NGC 650CS	(14000	(10200)	(260)	...	1.10	1.31	0.069[h]	0.067	...	6.3	0.136:[h]	0.50[h]	0.09
W	(13600)	(10200)	(260)	...	1.53	1.51	0.091[h]	0.061	...	7.4	0.152:[h]	0.50[h]	0.11
NGC 1360A[i]	16500	...	(50)	...	...	0.65	...	.082	...	...	≥ .08	...	...
B	16500	...	(50)	...	...	0.64	...	.055	...	...	...	...	...
NGC 2438C	(15300)	(10200)	...	430	0.16	0.65	0.046[j]	0.091	...	...	0.137:[j]	0.34[j]	0.09
W	(10900)	(10200)	...	170	1.51	2.84	0.154[j]	0.019	...	5.4	0.17:[j]	0.34[j]	0.21
NGC 3587	(11000)	(10200)	...	120	0.75	3.08	...	0.020	...	4.7	...	0.28[k]	0.11
NGC 4361	19400	(10200)	(150)	...	...	0.14	...	0.105	...	...	≥0.105	...	...
NGC 6026	(15100)	(10200)	(320)	...	...	1.13	...	0.088	...	...	...	...	...
NGC 6072	(12700)	11400	1530	...	(1.16)	2.64	0.111	0.047	0.51	5.4	0.158	0.44	...
NGC 6781A	10000	9000	180	...	2.68	3.39	0.102	...	0.96	6.1	0.102	0.36	0.16
B	14700[l]	10400	520	...	1.82	1.04	0.132	0.006	0.64	2.0	0.138	0.35	0.13
NGC 6842	17300[m]	(10200)	(280)	...	0.059	0.46	0.101	0.044	0.017	0.8	0.145	0.29	...
NGC 7094[b]	(17700)	...	(50)	...	...	0.51	...	0.134	...	...	>0.13	...	...
NGC 713924"N	(10300)	(10200)	(110)	...	1.20	1.92	0.127	...	0.76	3.1	0.127	0.63	0.25
CS	(11300)	(10200)	...	290	1.75	2.73	...	0.024	...	5.5	...	...	0.12
25"W	(10300)	(10200)	...	130	3.01	...	0.123	...	...	...	0.123	...	...
NGC 7293K	(11800)	(10200)	(70)	...	(1.28)	2.23	...	0.032	0.22	(5.0)	...	(0.17)	...
E	(11600)	(10200)	(70)	...	...	2.58	...	0.027	0.21	3.4	...	...	...
PC 21	12400	(10200)	(760)	...	0.041	1.77	0.034:	0.102	...	...	0.136	...[n]	...
Pu 1	(10300)	(10200)	(55)	...	3.13	1.34	...	...	0.66	4.5	...	0.21	0.19
PW 1	(10300)	(10200)	(75)	...	...	1.03	...	...	0.43	...	...	...	...
Sh1-89	(12200)	(10200)	140	...	0.74	1.36	0.156	0.038	1.04	2.6	0.193	1.4	...
VV1-2	(10300)	(10200)	420	...	(2.21)	...	...	...	0.16	2.2	...	0.07	...
VV1-4	(10300)	(10200)	840	1580	1.20	...	...	...	0.19:	...	...	0.16:	...
We 1	(10600)	(10200)	(>4)	...	0.038	3.53	...	0.013	...	4.1	...	...	...
We 2	(10300)	(10200)	(30)	...	2.51	1.15	...	...	1.00	3.7	...	0.40	...
We 3	(10300)	(10200)	(5)	...	...	0.80	...	...	1.14	...	...	...	...
We-5	(15800)	(10200)	(120)	...	...	0.27	...	0.100	...	...	≥0.100	...	...

[a] 15″E position only.
[b] Average of three positions.
[c] Region 2 only.
[d] Average of two positions; N/O from K83.
[e] Very uncertain because of companion star.
[f] Very unreliable line.
[g] Used in calculations.
[h] He^+ likely unreliable; O/H calculated from He/H = 0.108 derived from Aller and Czyzak 1983, from which O/H = 7.5×10^{-4} directly. N/O from K83; agrees with Aller and Czyzak 1983.
[i] Mean [O III] used for region A.
[j] He^+ likely unreliable; O/H calculated from He/H = 0.095 derived from Torres-Peimbert and Peimbert 1978, from which O/H = 6.5×10^{-4} directly; N/O from K83.
[k] N/O from K83.
[l] λ4363 is poor; T[O III] uncertain. If T = 10,300 K, O/H for region B agrees with that for region A.
[m] The line λ4363 is uncertain. If T_g = 12,400 K, appropriate to $I(\lambda 4686)$, O/H = 1.5×10^{-4}, $N_e^{2+}/O = 0.21$.
[n] C/O = 2.6.

and N/O, set as usual equal to N^+/O^+. If the He^{+2}/H^+ value is not known, we sum O^+/H^+ and O^{+2}/H^+ and give it in the O/H column as a lower limit. If He^{+2} is available, but He^+/H^+ is not, then He/H is assumed to be 0.11 and O/H is set in parentheses. If the ionization level of the nebula is high, and the O^{+3} correction is large (a factor of 2 or greater), we assume that it is too uncertain and leave the O/H column blank. If O^+/H^+ is based on [S II] λ6723 or [O I] λ6300, the brackets or parentheses are repeated around the N/O values. Finally, in the last column we list another ionic ratio, Ne^{+2}/O.

There are few opportunities for comparison. The agreement of N/O with K83 is reasonable; our new values should generally be superior. Our N/O for NGC 7293 is below that found by Torres-Peimbert and Peimbert (1987), and confirms their finding that Hawley's (1978) is to high. Our values for M2-55 and M3-3 are in qualitative accord with theirs, showing these objects' respective unenriched and highly enriched natures; quantitatively, we average 35% lower. Our line intensities for M2-55 agree well with theirs, but our Hα intensity for M3-3 is 20% higher. Our He/H values are more problematic; our measurements for NGC 650 and NGC 2438 are notably higher than those respectively made by Aller and Czyzak (1983) and by Torres-Peimbert and Peimbert (1978). That for NGC 650 agrees better with Peimbert and Torres-Peimbert (1987) but still averages 13% too high. Our data were derived from particular Steward runs that provided only one observation apiece, and which include no other nebulae, and we believe that theirs are superior. We adopt the lower results from Aller and Czyzak (1983) for NGC 650 and those of Torres-Peimbert and Peimbert (1978) for NGC 2438. However, for M2-55 our He/H is 20% lower than Torres-Peimbert and Peimbert (1987), while for M3-3 the values agree well. In a few instances we can compare results from two positions in the nebula, knowing that total abundances should be the same. The ionic results are in reasonable accord with expected stratification. Note that although He^{2+}/H^+ decreases from the center into the lobes for M2-55, N/O remains the same and O/H shows little change. The N/O ratios are the same for the two regions of NGC 6781, but the O/H ratios differ notably, probably a result of an erroneous electron temperature. NGC 7139 shows good agreement between the two values of He/H. See the footnotes to Table 10.

e) Central Star Temperatures and Luminosities

Our data can be used to derive Zanstra temperatures for the central stars, where we employ the code described by K83. The most critical parameters here are the stellar magnitudes, which are not available for all the objects. Known values of B and/or V are given in the second and third columns of Table 11, with references ("Ref") in the adjacent column, keyed at the bottom. Magnitudes are taken from Table 7 only when no others are available, since Figure 1 indicates that ours may be somewhat too faint between $V = 17$ and 22 mag. In accord with the comparisons in Shaw and Kaler (1985), we add 0.5 mag to all of Kohoutek's values.

The He II λ4686 intensities used in the calculation of He II Zanstra temperatures are listed in the fifth column of Table 11. The global He II intensities from K83 and Shaw and Kaler (1989), enclosed in parentheses, are more appropriate than the values measured in this paper. We use the intensities given in Tables 2–6, which may be subject to moderate stratification effects, only when global values are not available. Our new intensities, however, are often useful in reducing the limits on $I(\lambda 4686)$ that appeared in K83: the new limits are substituted if they are lower. In some instances a better global view is obtained if we average our new data with those of others taken from Kaler (1976); these values are enclosed in brackets. The last of the necessary observational data, the Hβ fluxes and extinction constants, are taken from Table 8. The results, T(H) and T(He II), are presented in the sixth and seventh columns of Table 11. Temperatures derived from the surface brightness fluxes of Table 8 are much less reliable than those found from global fluxes and are enclosed in parentheses; an error of 0.4 in log $F(H\beta)$, which is quite likely, can produce errors in temperature of typically 15%–25%.

We see that, with very few exceptions, T(He II) > T(H), consistent with the idea that the nebulae are optically thick in the He^+ Lyman continuum but thin in that of H^+ (which leads to an undercount of ionizing photons). Keep in mind the possibility that the stars might possess an ultraviolet excess that renders T(He II) greater than the effective temperature (Henry and Shipman 1986; Méndez *et al.* 1988). However, the fact that the distribution of T(He II)/T(H) approaches unity as a limit is consistent with a distribution in optical depth (see K83 and Kaler and Jacoby 1989). Consequently, we identify T(He II) with the effective temperature, unless T(H) is greater than T(He II), in which case we suggest an average (the stellar magnitude is probably at fault). We give luminosities, in units of $L_\odot$, in the eighth column, based on the distances of Table 8. These are also derived from He II, unless again T(H) > T(He II), for which case we use an average of L(H) and L(He II) in accord with the comment above. Occasionally both L(H) and L(He II) are given, separated by a hyphen. In several instances (see the footnotes to Table 11) we adopt crossover temperatures and luminosities from Kaler and Jacoby (1989). Again, these are derived for optically thick nebulae by determining the stellar magnitude needed to force equality between T(H) and T(He II). These objects are considered to be thick on the basis of strong [O II] and [N II].

The adopted temperatures and luminosities in Table 11 are assigned a complex set of limits:

1. If $I(\lambda 4686)$ is an upper limit, so are T and L (A1, A5, A8, A9, A18, A59, A62, A80, K1-8, K1-9, K1-13, K1-20, K1-22, Pu 1, PW 1, VV 1-2, VV 1-4, We 2).
2. If B or V are lower limits, so is T, but L is an upper limit (We 1).
3. If $I(\lambda 4686) > 90$, the nebula is assumed to be optically thin in the entire Lyman continuum, and T and L are both lower limits (A15, A20, A36, A72, Ba 1, K1-14, K3-27, NGC 246, NGC 1360, NGC 4361, NGC 7094, We 5).
4. If T(H) is within 10% of T(He II), the nebulae are probably ionization-bounded and the distances, radii, and luminosities are upper limits (A80, K1-7, K1-13, K1-22, NGC 650, NGC 3587, NGC 6072, NGC 7293).
5. If there are no magnitudes and $I(\lambda 3727) > 100$ [or, in the absence of λ3727, if $I(\lambda 6583)/I(H\alpha) > 1$], the nebula is considered thick, crossover temperatures are taken from Kaler and Jacoby (1989), and distances and luminosities are considered upper limits (A82, He 1-6, K1-1, K3-74, K3-91, M2-55, M3-3).

IV. DISCUSSION

a) Especially Interesting Objects

Before proceeding further, we point out some nebulae that are of particular interest relative to a variety of special categories. First, Lo 4 and We 5 appear to be new members of the

TABLE 11

ZANSTRA TEMPERATURES AND LUMINOSITIES

Nebula	B	V	Ref	I(λ4686)[a]	10^{-3} T(H)[b]	10^{-3} T(He II)[b]	$L/L_{\odot}$	Status	M_c
A 1	19.9	...	1	<55	(31)	(<77)	<1400	H	0.55
A 2	20.0	...	1	(61)	88	132	170	D	0.69
A 4	19.5	...	1,2	(23)	70	99	120	D	0.58
A 5	21.4	21.4	3	<75	89	<139	<24	D	1.09
A 8	19.9	...	1,2	(<30)	46	<87	<46	Q	0.55
A 9	24.5	23.5	3	<50	(91)	<131	<49	D	0.90
A 12	19.1	...	1	38	111	135	290	D	0.65
A 15	15.41	15.72	1	(128)	27	>76	>12	LHE	...
A 18	21.36	20.90	3	<25	69	<106	<73	D	0.63
A 20	16.29	16.56	1	(149)	39	>99	>580	LHE	...
A 33	...	15.7	4	(58)	51	99	105	D	0.59
A 36	11.18	11.51	1	(118)	26	>73	>660	LHE	...
A 59	22.21	21.15	3	<25	85	<113	<89	D	0.65
A 62	18.7	...	2	(<20)	64	<96	120-390	D	0.55
A 70	18.7	...	1,2	(46)	62	104	95	D	0.61
A 72	15.79	16.12	1	(111)	39	>94	>340	LHE	...
A 75	17.6	...	1,2	(81)	51	106	900	K	0.56
A 80	19.38	19.61	3	<25	123[c]	<135[c]	26[c]	D	1.05
A 82[d]	...	...	...	(15)	...	116[d]	<58[d]		>0.72[d]
A 84	18.67	18.49	1	(17)	92	107	28	D	0.79
Ba 1	17.6	...	2	(90)	41	>94	>610	LHE	...
Hel-6[e]	...	...	...	17	...	121[e]:	<220[e]:	D	>0.62[e]:
IC 5148	...	15.2	5	45	(40)	(84)	330	D	0.55
Jn 1	15.72	16.13	6	(50)	49	95	55	D	0.60
Kl-1[f]	...	...	...	33	...	150[f]	<36[f]	D	>1.08[f]
Kl-3	20.5	...	2	28	87	118	930:	K	0.57
Kl-7	19.8	...	1,2	(13)	107	108	47	D	>0.69
Kl-8	17.3	...	2	<35	28	<68	<2650	H	0.57
Kl-9	19.1	...	2	<35	(43)	(<85)	<150	D	0.55
Kl-13	18.80	18.94	1	<50	204[c]	<195[c]	55[c]	D	1.2
Kl-14	...	16.4	5	(160)	31	>86	>520	LHE	...
Kl-17	19.1	...	2	63	(44)	(93)	220	D	0.55
Kl-20	20.6	...	2	(<10)[g]	67	<87	22-45	D	0.59
Kl-22	...	17.9	5	<10	91	<97	14-18	D	0.79
K3-27	...	17.1	5	(92)	43	>97	>1600	LHE	...
K3-73	20.8	...	7	20	(98)	(112)	63	D	0.69
K3-74[h]	...	...	...	36	...	160[h]	<50[h]	D	>1.07[h]
K3-86	...	22.75	8	71	(81)	(132)	380	D	0.63
K3-91[i]	...	...	...	37	...	171[i]	<300[i]	D	>0.77[i]
K3-92	...	20.6	7	14	46	78[j]	1020[j]	H	0.55[j]
M2-51	19.2	...	7	(13)	89	102	200	D	0.56
M2-53	21.2	...	7	26	82	111	510	K	0.56
M2-55[k]	...	...	...	(4)	...	85[k]	<110[k]	D	>0.55[k]
M3-2[l]	16.88	16.96	9	(80)	32	80[l]	4700[l]	H	0.60[l]
M3-3[l]	...	...	...	11	...	105[l]	<205[l]	D	>0.57[l]
M4-11	17.9	18.0	3	66	(60)	110	1100	H	0.56
NGC 246	11.58	11.95	6	(121)	33	>85	>880	LHE	...
NGC 650	...	17.5	4	(54)	162	175	230	D	>0.89
NGC 1360	10.86	11.35	10	(99)	34	>84	>570	LHE	...
NGC 2438	...	17.88	5	(41)	131	147	140	D	0.78
NGC 3587	15.59	16.04	6	(11)	112[c]	107[c]	45[c]	D	>0.70
NGC 4361	12.74	13.04	6	(115)	42	>98	>1040	LHE	...
NGC 6026	13.35	13.29	9	(56)	26	>68	>7440	LHE	...
NGC 6072	18.97	18.47	9	(25)	163[c]	149[c]	340[c]	D	>0.69
NGC 6781	16.8	...	2	[13]	75	95	230	D	0.55

TABLE 11—*Continued*

Nebula	B	V	Ref	I(λ4686)[a]	10^{-3} T(H)	10^{-3} T(He II)	$L/L_\odot$	Status	M_c
NGC 6842	16.8	...	2	42	50	94	900	H	0.55
NGC 7094	13.36	13.61	6	(116)	26	>72	>1600	LHE	...
NGC 7139	...	18.72	8	[14]	94	105	79	D	0.63
NGC 7293	13.09	13.43	6	(10)	116[c]	107[c]	36[c]	D	>0.76
Pu 1	21.13	21.16	3	<18	(64)	<93	<46	D	0.60
PW 1	15.4	...	11	<33	69	<105	4-12	D	0.99
Sh1-89	19.6	...	2	39	(126)	(145)	270	D	0.69
VV1-2	14.4	...	2	<16	30	<65	<930	?	...
VV1-4	11.9	...	2	<10	28	<59	<4400	?	...
We 1[m]	>21.1	...	12	15	(>28)	(>61)	<44	D	>0.55
We 2	21.33	21.87	3	<100	(65)	<125	<100	D	0.70
We 3	21.24	21.01	3	...	(64)	...	>76	D	0.60
We 5	18.9	...	12	95	32	>82	>1700	LHE	...

NOTE.—In "Status" column, H = horizontal evolutionary track; D = descending evolutionary track; LHE = large, high-excitation nebula; K = near the knee of the 0.55 $M_\odot$ track; ? = status unknown.

[a] Values not enclosed; this paper; parentheses: global values from Kaler 1983, or for NGC 6026, NGC 6072, and M3-2 from Shaw and Kaler 1989; brackets: averages from this paper and data in Kaler 1976.

[b] Values in parentheses derived from surface brightness fluxes.

[c] Use mean of T(H) and T(He II); luminosity is mean of L(H) and L(He II).

[d] Crossover for A82, predicted $V = 19.1$ (Kaler and Jacoby 1989).

[e] Crossover for He 1-6, predicted $V = 20.30$.

[f] Crossover for K1-1, predicted $V = 21.5$.

[g] If $I(\lambda 4686) = 17$, from this paper, $T = 94{,}000$ K, $L = 55\ L_\odot$.

[h] Crossover for K3-74, predicted $V = 23.95$.

[i] Crossover for K3-91 and flux of Table 9, predicted $V = 26.12$.

[j] Crossover values are $T = 115{,}000$ K, $L = 240\ L_\odot$, $V = 23.31$, but M_c is still $0.55\ M_\odot$.

[k] Crossover for M2-55, predicted $V = 19.2$.

[l] Crossover for M3-3, predicted $V = 20.33$.

[m] Extinction not known.

REFERENCES.—(1) Abell 1966; (2) Kohoutek, in Perek and Kohoutek 1967 (0.5 mag added as in Shaw and Kaler 1985); (3) Kwitter, Jacoby, and Lydon 1988; (4) Cudworth 1973 (these are binary nuclei); (5) Kaler and Feibelman 1985 (corrected for the new extinctions); (6) Shao and Liller 1973; (7) this paper; (8) Jacoby and Kaler 1989; (9) Shaw and Kaler 1989; (10) Shaw and Kaler 1985; (11) Purgathofer and Weinberger 1980; (12) Weinberger 1977.

class of large high-excitation objects (Kaler 1981, 1983) whose helium is fully doubly ionized, and are optically thin even in the He^+ Lyman continuum. They are seen in Table 11 to have the requisite high He II Zanstra temperatures (which are, again, lower limits). Second, note that some other objects have Zanstra temperatures that are quite high, particularly K1-13, NGC 650, NGC 2438, NGC 6072, and Sh 1-89, all of which approach or exceed 150,000 K. The crossover temperatures for K1-1, K3-74, and K3-91 are in the same league. The temperature for Sh 1-89, however, is based on an unreliable flux.

Third, and more important, we identify a number of nebulae that fall into Peimbert's (1978) type I, those prominently enriched in either helium or nitrogen by dredge-up processes that took place in the progenitor star (Becker and Iben 1979, 1980; Renzini and Voli 1981). The definition is rather loose: Peimbert (1978) originally used He/H $\geq$ 0.14 or N/O > 1, and then Peimbert and Torres-Peimbert (1983) changed it to He/H $\geq$ 0.125 or N/O $\geq$ 0.5. In order to allow for errors and to be certain that we identify true type I objects, we choose He/H > 0.15 or N/O $\geq$ 0.8. This enriched set, based on N/O alone, includes A5, A69, A80, K1-1, K1-9, K1-13, M3-2, M3-3, and Sh 1-89 (though note that the O^+/H^+ for A69 and K1-9 are based on the [S II] line strength). We also derive a concomitantly high He/H ratio for K1-1, M3-2, and Sh 1-89, and declare M4-11 also to be Type I based on He/H alone. A5 is a curiosity, as it appears to hold the current record for the [N II] λ6583/Hα intensity ratio, at 7:1!

Several of these type I nebulae are morphologically distinctive: A5, A80, and K1-1 are distinctly binebulous, following the correlation presented by K83. (Others, however, are not binebulous: we do not consider morphology here, since with new techniques constantly providing better images the subject is in too great a state of flux.)

One other interesting nebula comes close to falling into two special categories. A20, a large, high-excitation nebula, has $He^{+2}/H^+ = 0.13$. If there is any significant singly ionized helium present, He/H could be quite high. We will look further at abundance correlations in § IV*c*.

b) Distribution on the log *L*–log *T Plane*

Much of the discussion of this paper involves the positionings of the stars on the log *L*–log *T* plane and an evaluation of their core masses. We plot the stars on the log *L*–log *T* plane in Figure 5 according to the precepts of § II*e*, i.e., we adopt T_z(He II) and L_z(He II) unless T(H) > T(He II), under which conditions we assume averages of results from H and He II. Calculations that use the surface brightness fluxes are indicated in the figure by small symbols. Arrows indicate limits. This diagram uses the same scale as Figures 11 and 12 in K83, with which it can be directly compared. The evolutionary

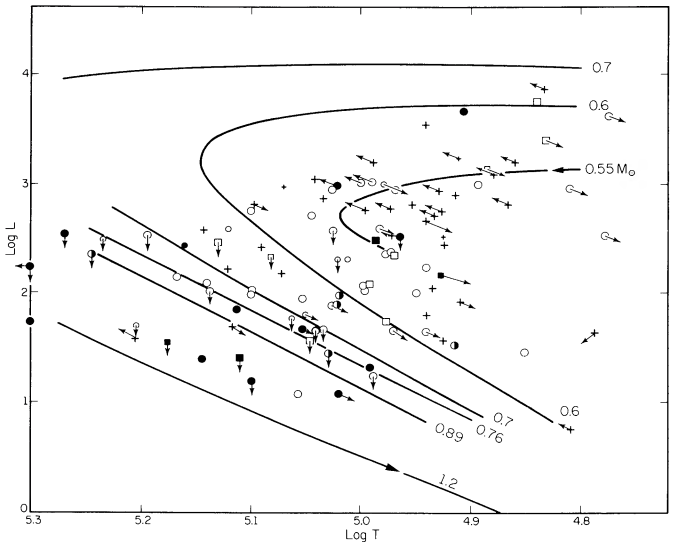

FIG. 5.—Planetary nuclei on the log L–log T plane, supplemented by data taken from Kaler (1983) and elsewhere as described in the text. *Filled symbols*: N/O $\geq$ 0.8, or He/H > 0.15; *half-filled symbols*: 0.8 > N/O $\geq$ 0.5; *open symbols*: N/O < 0.5; *plus signs*: no abundance data. The smaller symbols denote crossover values and those derived from surface brightness fluxes. *Solid lines*: evolutionary tracks from Wood and Faulkner (1986) for $\phi = 0.5$, mass-loss type A, except for 1.2 $M_\odot$, which is from Paczyński (1971).

tracks for 0.6, 0.7, 0.76, and 0.89 $M_\odot$ are taken from Wood and Faulkner (1986) for case A mass loss and $\phi = 0.5$. That for 0.55 $M_\odot$ is from Schönberner and Weidemann (1981), and the one for 1.2 $M_\odot$ is adopted from Paczyński (1971).

In order to increase the number of data points and the reliability of our conclusions, we add objects from K83 that are not covered by this study, and a few planetaries from Shaw and Kaler (1989) that fit our criteria. We except the large, high-excitation objects from these papers, since they add nothing new to the diagram.

The points are distributed from a low of about 55,000 K (which is an upper limit) to 236,000 K. The latter (BV 1) runs off the figure to the left. The majority have $L < 1000\ L_\odot$, consistent with relative old age and evolutionary placement on the descending tracks (the lowest luminosity is only a few times solar). The major exceptions are primarily the set of large high-excitation objects that generally fall inside the knee of the 0.55 $M_\odot$ track, and that actually lie up and to the left somewhere along the projecting arrows: provided that the distances are right. Their real evolutionary status is uncertain, except that two of them, A30 and A78 (not plotted here), are thought to have undergone thermal pulses when they were previously on descending tracks, and are retracing their paths for the second time (Iben *et al.* 1983). Other exceptions include a few nebulae with stars that still appear to be evolving to the left along horizontal evolutionary paths: A1, K1-8, K3-92, M3-2, M4-11, NGC 6842, and (if they are indeed planetaries) VV 1-2 and VV 1-4. Yet another group is near the knee of the 0.55 $M_\odot$ track. These evolutionary locations are indicated by letters in the "status" column of Table 11, with the abbreviations keyed at the bottom.

We can rather simply estimate the core masses, M_c, by interpolating (nonlinearly) between the tracks; the results are listed in the last column of Table 11 in solar units, and in Table 12 for the K83 and Shaw and Kaler (1989) objects. In both cases, 0.55 $M_\odot$ is taken as a lower limiting value. Again, we must contend with limits. If D and L are upper limits, as they are for optically thick nebulae, so are the M_c. However, if $I(\lambda 4686)$ is an upper limit, which renders *both* T and L upper limits, the locus along which a star lies points down and to the right, roughly parallel to the descending tracks, so that if the star is cooling, M_c will be approximately correct. Errors in core mass will be produced by errors in T and L, which are dependent on the input parameters, notably log $F(\mathrm{H}\beta)$ and V. Most of the fluxes are quite well known, with insignificant errors, but those derived from the surface brightnesses are subject to errors of ± 0.4 in the log or even more, which will yield core-mass errors of the order of 0.05–0.10 at core masses of 0.6–0.7 $M_\odot$. Even larger errors are possible. Errors in V, typically of the order of 0.2 mag, yield core-mass errors that are considerably smaller.

It is also hard to evaluate the effect of systematic errors in the Shklovsky distances, which are based upon a common nebular mass. If nebular mass actually scales directly with core mass, as seems intuitively likely, then we will systematically underestimate the distances of the higher mass stars, thus placing them too high in the mass distribution. At least, however, the *relative* core masses should still be accurate, which is what is needed for the analyses below. We will proceed as if the core masses in Table 11 are correct, but the reader should keep in mind that they might well be scaled downward according to an unknown function but with relative placement intact. The core masses will also be systematically shifted if we use other theoretical tracks.

We see, as in K83, that the stars do not clump tightly about the 0.6 $M_\odot$ track as they did in Schönberner's (1981) study; here they spread out to 0.7 $M_\odot$ and as high as 1.2 $M_\odot$. The distribution seems to be wider (especially considering the limiting arrows) in core mass than the narrow white dwarf distribution found by Koester, Schulz, and Weidemann (1979) and by others. A histogram (without regard to limits) of the masses shows that about 40% of the cooling cores have masses greater than or equal to 0.7 $M_\odot$, and 17% are larger than 0.8 $M_\odot$, showing at least that large core masses may well be common. If we take limits into account, the percentages would likely be larger. A difference between the distribution of planetary nuclei and that found for white dwarfs is not surprising, since planetary nuclei are only designated as such if there are nebulae around them, and detectability depends on expansion velocities and evolutionary time scales. Thus, natural (and unknown) selection effects are present. Only a volume-limited sample, which ours is definitely not, can give the true core-mass distribution.

c) *Alterations in Element Abundances*

Next we look at the alterations—enrichments and depletions—that appear in the planetary nebulae as a result of nuclear processing in the progenitor stars. The relations among the alterations, and between enrichments and core masses, provide critical tests of mass loss and dredge-up theory for the planetary progenitors. The matter is discussed at some length by K83 and Kaler (1985*b*). Briefly, giant stars are expected to enrich their outer layers—the gases that will form the planetaries—in helium, nitrogen, or carbon as a result of various processes that dredge up material from the core. The N/O and He/H ratios are expected to grow larger with increasing initial stellar mass (Becker and Iben 1979, 1980; Renzini and Voli 1981), in principle allowing us to infer such mass from the nebular composition. Furthermore, the initial and remnant masses are directly related to one another (Iben and Truran

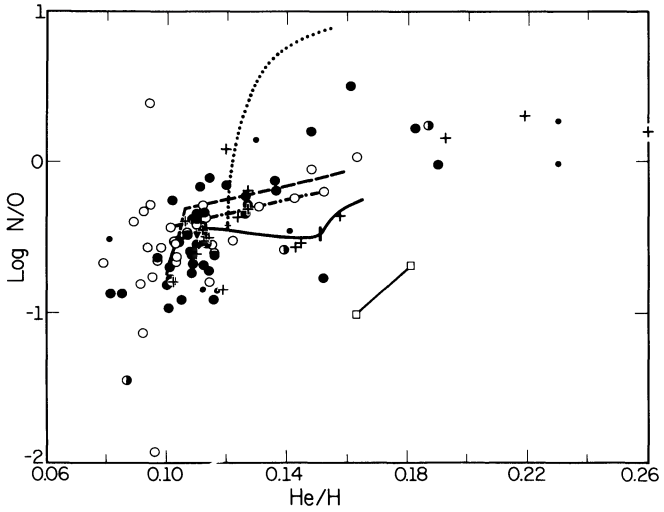

FIG. 6.—N/O vs. He/H taken from Kaler (1985), overplotted with our new data (*plus signs*) as described in the text. The small plus sign has a large error. The open and closed circles represent extant data for Populations I and II, respectively. *Solid line*: predictions for third dredge-up; *dotted line*: third dredge-up with hot bottom burning for $\alpha = 2$; *dashed line*: third dredge-up with conversion of C to N in the envelope at one-half the maximum rate; *dot-dash line*: second dredge-up only. All calculations are from Becker and Iben (1980), except for a hot bottom burning case, which is from Renzini and Voli (1981).

1978; Kwok 1983). As a result, He/H and N/O should correlate with core mass, and consequently with the location of the planetary nucleus on the log L–log T plane (see Renzini 1979).

i) *Nitrogen and Helium Enrichment*

We present our new data (N/O vs. He/H) in Figure 6 against the background of the previous correlation (which used all extant data) published by Kaler (1985*b*). The two objects for which we earlier cited disagreement with previous abundance determinations (NGC 650 and NGC 2438) are excluded. We see a good fit between the two data sets (old and new), and again the three new really extreme objects. But the data do not exclusively distinguish any of the possible theoretical scenarios. The scatter is large and crosses over all the possibilities discussed by Becker and Iben (1980) and Renzini and Voli (1981), including all the second and third dredge-up possibilities and hot bottom (envelope) burning (see the legend to Fig. 6). In addition, note the objects that extend to the right far beyond the termination of the theoretical curves. The spread appears too large to be caused by observational errors, and we suggest that it is real. We speculate here that some progenitor stars in fact operate only through the second dredge-up, while others undergo a third with or without hot bottom burning, triggered by an as yet unknown mechanism. The great range of helium and nitrogen abundances that extend to much higher enrichments than those predicted by theory is confirmed by our new work and remains to be explained.

ii) *Nitrogen Enrichment and Core Mass*

Now let us look at the N/O ratios (Table 10) as displayed on the log L–log T plane in Figure 5. Supplementary values are taken from K83 and Kaler (1985*a*), for the highly enriched object BV 1 from Kaler, Chu, and Jacoby (1988), and for Ym 29 from Kwitter, Jacoby, and Lawrie (1983). All the supplementary objects are listed, with references to N/O, in Table 12. Stars for which there are no nebular N/O data are plotted as crosses, the others as circles, filled according to nebular N/O: open, $0 < \mathrm{N/O} < 0.5$; half-filled, $0.5 \leq \mathrm{N/O} < 0.8$; filled, $\mathrm{N/O} \geq 0.8$ (i.e., Peimbert type I as defined here). In addition, the nebula with He/H > 0.15 but with unknown N/O (M4-11) is considered to be type I also, and is represented by a filled symbol.

K83 noted weak support for the expected correlation between N/O and core mass. We see a similar tendency in

TABLE 12

ADDITIONAL DATA FOR LARGE OR TYPE I NEBULAE

Nebula	M_c[a]	Status	10^4 O/H	N/O	Notes
A3	0.55	H	...	...	
A6	0.55	D	...	...	
A13	0.59	D	...	...	
A16	0.59	D	...	...	
A24	>0.72	D	0.83	>2.7	1, 2
A28	0.59	D	...	...	
A31	1.04	D	2.1	0.40	2
A34	0.59	D	...	...	
A39	0.55	D	...	...	
A46	0.55	Q	...	...	
A50	0.71	D	4.4	0.40	2
A53	0.56	T	...	...	
A65	0.55	D	2.2	0.31	2
A71	0.78	D	1.4	2.4	2
BV 1	1.05	D	3.0	1.45	3
BV 3	0.55	D	...	...	
Hb 5	...	...	6.7[b]	2.16	4
He 2-109	0.55	H	...	...	5
He 2-132	0.58	H	...	...	5
Hu 1-2	...	...	2.2[b]	1.43	6
IC 972	0.56	D	4.6	0.30	2
IC 1454	0.59	D	5.6	0.36	7
IC 4406	0.57	D	5.8	0.48	2
K2-1	0.74	D	...	...	
K2-2	0.56	D	...	...	8
K3-61	...	...	3.2	4.1	4
NGC 2440	>0.9	...	5.1	2.4	9, 10
NGC 2474	0.75	D	3.5	1.2	2
NGC 2818	>1.0	...	3.5	1.10	11, 10
NGC 4071	>0.63	D	...	...	5
NGC 6058	0.61	H	3.5	0.32	7
NGC 6302	>0.74	...	3.1[b]	5.2[c]	12
NGC 6445	>0.84	D	5.2	1.2	2
NGC 6563	0.55	D	<1.6	>1.0	5, 7
NGC 6720	0.60	D	6.2	0.35	2, 13
NGC 6765	0.55	H	...	...	
NGC 6772	0.62	D	...	...	
NGC 6778	...	...	5.7	1.1	14
NGC 6853	0.76	D	8.4	0.36	2, 15
NGC 6894	>0.55	D	6.2	0.99	2, 4
NGC 7048	0.65	D	...	...	
PB 6	...	...	4.1[b]	1.65	10
PW 1[d]	0.99	D	3.27	1.16	2
Sh 2-71	...	...	2.4	6.4	2
Ym 29	>1.08	D	3.0	0.96	16

NOTES.—(Two numbers refer respectively to mass and composition.) (1) $T < 113{,}000$ K, $L < 47\ L_\odot$ from Cudworth's 1973 magnitude; (2) O/H, N/O calculated and/or taken from K83 and references therein; (3) Kaler, Chu, and Jacoby 1988; Jacoby and Kaler 1989; (4) from data in Aller and Keyes 1987; (5) from data in Shaw and Kaler 1989; (6) from data in Aller and Czyzak 1979; (7) abundances from Kaler 1985*a*; (8) $T = 71{,}000$ K, $L = 29\ L_\odot$ from Kwitter, Jacoby, and Lydon's 1988 magnitude; (9) $T = 217{,}000$ K, $L < 450\ L_\odot$ from Jacoby 1988 and Heap and Hintzen 1989; data also taken from Gutiérrez-Moreno, and Cortés 1985; (10) from data in Torres-Peimbert and Peimbert 1978; (11) from data in Dufour 1984; (12) from data in Aller and Czyzak 1978; (13) Barker 1980; (14) from data in Aller and Czyzak 1983; (15) Barker 1984; (16) O/H from Kwitter, Jacoby, and Lawrie 1983, N/O mean from that paper and K83.

[a] M_c from data in K83 unless otherwise specified.

[b] Correction for O^{+3}, and so on, high (≈ 2).

[c] High density.

[d] See Tables 10 and 11.

Figure 5, in that there is a concentration of type I nebulae toward higher core mass. But we can see this relationship better by plotting N/O from Table 10 directly against core mass from Table 11, which we do in Figure 7. Here we add three other type I objects, NGC 2440, NGC 2818, and NGC 6302 (see Table 12), whose core masses were found from the temperatures and luminosities given by Kaler and Jacoby (1989); these nebulae are all smaller than 0.15 pc, but the stars still are on descending tracks, so that even though optically thick, the core masses are lower limits. The figure shows some significant tendencies. First, the nebulae with low N/O strongly concentrate toward lower core mass: of the 45 non–type I objects (N/O < 0.8), all but three have central stars under 0.8 $M_\odot$. The median N/O of this densely packed group is about double the solar value of 0.15 (Ross and Aller 1976). It would appear that most nebulae are at least mildly enriched in N, as expected from Becker and Iben (1979, 1980). In contrast, the highly enriched type I objects show a much broader distribution in M_c, with 10 nebulae having cores both above and below 0.8 $M_\odot$. Note, however, that of the type I objects with $M_c < 0.8\ M_\odot$, two are located by uncertain surface brightness fluxes, and four are placed only as lower limits. If we exclude these six, then the preponderance of type I objects falls toward higher core mass as theoretically expected. If we quarter the diagram at M_c = N/O = 0.8 and exclude the uncertain points based on surface brightness data, we find the ratio of high to low N/O at low core mass to be 8:38, whereas it is 10:2 at high core mass. A χ^2 test shows the correlation to be significant at well above the 99% level. We consequently see a strong and convincing relation between nebular N/O and stellar mass. This relation is supported by a similar correlation found by Kaler and Jacoby (1989) between N/O and central star temperature for an independent set of optically thick planetaries

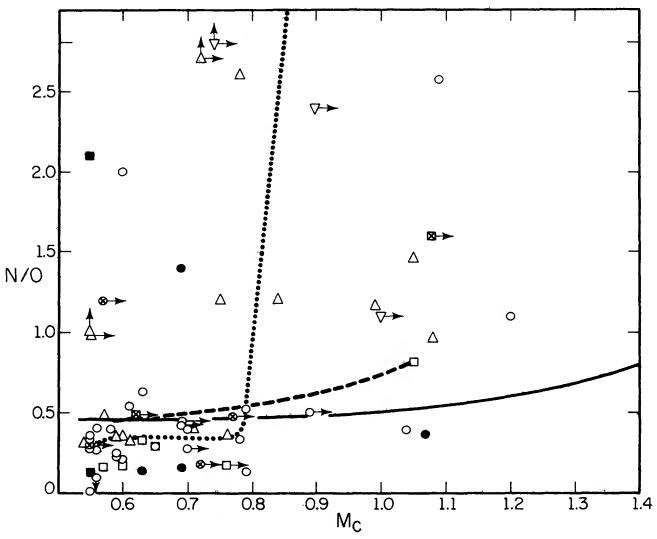

FIG. 7.—N/O ratios plotted against core mass. *Open circles*: this paper, where O^+ is from [O II] λ3727; *squares*: this paper, where $I(\lambda 3727)$ is estimated from [O I] or [S II]; *open symbols with crosses*: M_c derived from crossover temperatures; *triangles*: objects from K83; *inverted triangles*: small type I objects on descending tracks; *filled symbols*: core masses derived from surface brightness fluxes. *Solid curve*: prediction from Becker and Iben (1980) (third dredge-up with C to N conversion) and initial-final mass conversion of Iben and Truran (1978); *dashed curve*: same, but with Kwok's (1983) mass conversion; *dotted curve*: Renzini and Voli's (1981) envelope burning for $\alpha = 2$ and Kwok's mass conversion.

that are also on descending evolutionary tracks: as T_z(He II), and hence core mass, rises, so does N/O. There seems to be no question that core mass and nebular nitrogen enrichment are strongly related. However, the actual form of the correlation is still unclear. It does not seem to be smooth or monotonic, although such a correlation could be masked by errors in distances and hence core mass. Rather, above 0.8 $M_\odot$ (or perhaps lower) there is suddenly a greatly increased possibility for high N/O. Nevertheless, it appears that high N/O might occur at low core mass, and low N/O at high core mass. Refined core masses (from improved distances) are clearly needed to resolve the matter and to see whether or not the great spread in N/O for a given core mass is real.

We compare the observations with some predictions. If we adopt Becker and Iben's second dredge-up calculations (which give the highest N/O, excluding the hot bottom burning possibility) and Iben and Truran's (1978) relation between initial and final masses, we get the solid curve in Figure 7, which increases to a maximum of 0.8, far too low, only at a core mass of 1.38 $M_\odot$, which is far too high. We do somewhat better by using Kwok's (1983) initial-final mass relation, which incorporates more mass loss and which is shown by the dashed curve. This one at least approaches the collection of points around 1 $M_\odot$. The calculations by Renzini and Voli (1981) for envelope burning (for a mixing length $\alpha = 2$ as given in their Fig. 10) combined with Kwok's mass relation produces the dotted curve in the figure. This last shows a sudden onset of high N/O at about $M_c = 0.8\ M_\odot$, rather similar to what we observe. However it does not explain the spread of moderately high N/O at higher core mass; for these, envelope burning predicts a much higher N/O than we see. It seems possible that envelope burning operates at lower mass, $M_i \approx 3$–4 ($M_c \approx$ 0.75–0.9) but not at higher mass ($M_i \approx 5$, $M_c \approx 1$). Even then, second or third dredge-up appears to be more efficient than expected. These results are vaguely consistent with the large spread seen in Figure 6. On the basis of binary companions to three planetary nuclei, Peimbert and Serrano (1980) suggest that type I nebulae develop from stars with masses greater than 2.4 $M_\odot$. From Figure 7 and Kwok's mass relation we find a somewhat higher value of about 3.2 $M_\odot$ if the onset of high N/O is at $M_c = 0.8\ M_\odot$. These discussions of course are dependent upon uncertain distances.

iii) *Oxygen Depletion*

Torres-Peimbert (1983) found that O/H was anticorrelated with N/O in type I Galactic planetaries, but the observational data were sparse, the scatter large, and the relation needed additional investigation. Aller (1983) had somewhat earlier suggested that such a correlation existed for Large Magellanic Cloud objects. Such an effect can also be seen in Kaler's (1980) discusssion of O/H ratios, where extreme disk planetaries with high He/H have lowered O/H. Henry, Liebert, and Boroson (1989) have now more clearly confirmed that among planetaries of both Clouds, O/H decreases as N/O increases. Does this correlation then actually hold in the Milky Way? Apparently it does, but in a more complex manner that is not really obvious until the stars of higher mass are included.

We plot N/O against O/H from Table 10 as circles and squares in Figure 8. In order to increase the body of data, we add other large nebulae from K83. That paper did not list O/H ratios, so we calculated them from the data presented therein and list the results (with N/O) in Table 12 and plot them along with BV 1 as triangles in Figure 8. The symbols representing

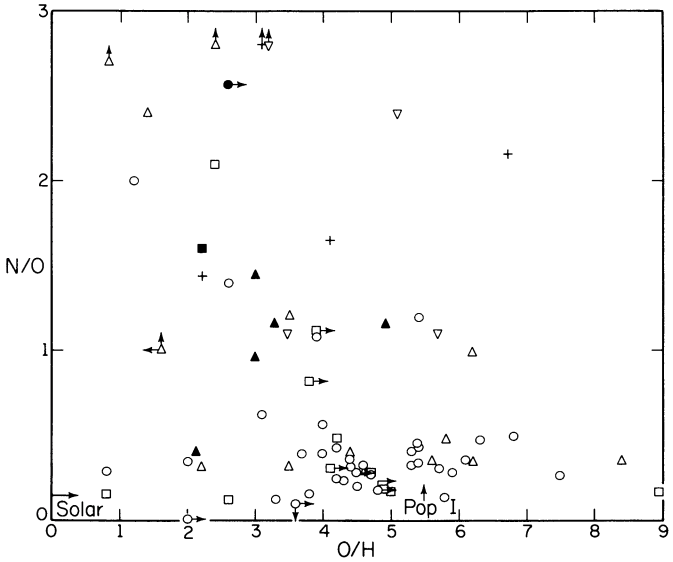

FIG. 8.—N/O plotted against O/H. The circles and squares respectively represent nebulae with O^+/H^+ derived from [O II] λ3727 or from [S II] or [O I]; *filled symbols*: $M_c > 0.8\ M_\odot$; *triangles*: O/H and N/O from K83; *inverted triangles*: supplementary type I objects (see text); *plus signs*: $He^{2+}/He^+ > 1$, O/H uncertain.

those nebulae with $M_c > 0.8$ are filled. We also adopt a small additional set of nebulae known to have N/O > 0.8, where we calculate O/H (or adopt values) from the references that accompany the results in Table 12 (inverted triangles in Fig. 8). Objects that display Population II characteristics (high velocity and great distance from the Galactic plane) are excluded from the supplementary set in order to produce a sample with similar initial starting conditions. The entire data set is calculated according to the precepts of Kaler (1985*a*), so that all objects can be properly compared. Four nebulae for which the correction for higher ionization stages of oxygen is greater than a factor of 2 are shown as plus signs; these are likely to be unreliable.

The median O/H for those nebulae with high nitrogen-to-oxygen ratios ($0.8 < N/O < 1.4$) is about 3.1×10^{-4}, noticeably less than it is for those with N/O < 0.8, for which it is 4.5×10^{-4}. For $N/O \geq 1.4$, the median O/H is only 2.5×10^{-4}, and if we drop the plus signs, it decreases to 2.4×10^{-4}. The correlation improves if we use only the data on large nebulae (i.e., if we ignore the crosses and the supplementary set represented by inverted triangles). Then, above N/O = 1.6, all objects have $O/H < 2.6 \times 10^{-4}$ (ignoring the uncertain limit on A5). It is interesting to note that the correlation appears to be genuine both for nebulae for which $M_c > 0.8$ (*filled symbols*) and for those with cores of lower mass (of which some could be higher because of uncertain distances). In summary, there seems to be little doubt that the correlation is present.

The correlation is actually even stronger than it at first appears. The spread in O/H for *low* N/O is almost certainly caused by the great intrinsic range in population type found in the Galaxy. Old and intermediate population nebulae have a wide range in O/H (e.g., Kaler 1980) and their progenitors have small initial mass, so that enrichment will not generally occur (although some lower mass stars may produce high nebulae with nitrogen; see Figs. 5 and 6). High nebular nitrogen (type I) appears generally to belong to the province of higher mass stars, those that produce the higher mass cores. The supplementary objects are in fact preselected in that direction. These will all be young Population I objects, and the O/H should then initially be high and relatively uniform. The likely starting point would be (from Kaler's 1980 groups 5a and 5b) about 5.5×10^{-4}, which is well above the O/H for enriched objects; only one (excluding an uncertain cross in the figure) falls above it. What we see, then, is the set of type I objects with relatively massive cores climbing out of the morass caused by a mixture of populations. The true correlation starts at $O/H \approx 5.5 \times 10^{-4}$ at low N/O and extends up and to the left to $O/H \approx 2 \times 10^{-4}$ at high N/O.

Unfortunately, we do not have good data to back up these speculations about population type for this particular sample. We can calculate distances Z from the Galactic plane easily enough from the Shklovsky distances, but radial velocities, a surer indication, are largely lacking. None of the nebulae with low N/O and O/H in Figure 7 has significantly high Z, and Schneider *et al.* (1983) list velocities for only two (only NGC 2438 would even marginally qualify as Population II, with $v_r = 76$ km s^{-1}). There are a few more velocities among the type I nebulae, and those for M3-2, M3-3, and NGC 2474 are rather high for disk objects, in absolute value between 84 and 95 km s^{-1}. The first two are subject to large error, however. As a consequence, some of the enriched objects could initially have had lower O/H. In spite of this lack of supportive population data, we feel that the reasoning behind the explanation of Figure 8 makes sense and is correct.

The correlation between O/H and N/O in the Galaxy is quite similar to that found in the Magellanic Clouds. The chief difference is in the large spread in O/H at low N/O for Galactic objects caused (presumably) by population effects. We compare the correlations in Figure 9, where we combine and

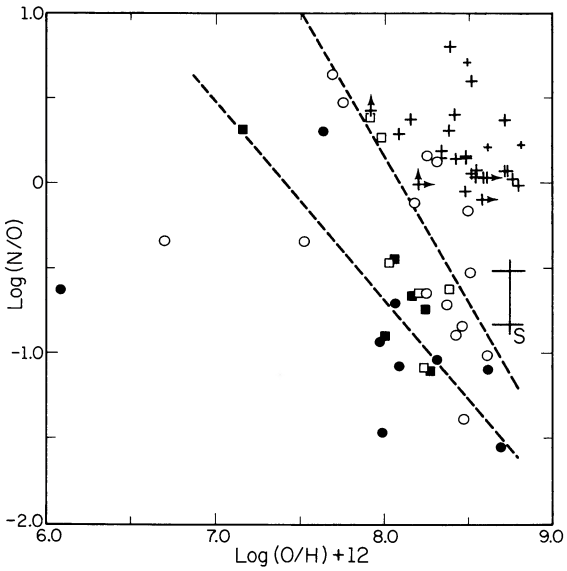

FIG. 9.—The log (N/O) vs. log (O/H) relations for planetaries in the Magellanic Clouds from Henry, Liebert, and Boroson (1989) (*filled and open symbols, respectively*) compared with that in the Galaxy for type I objects from this paper (*plus signs*). The smaller plus signs represent the objects with uncertain O/H seen as plus signs in Fig. 8. Dashed lines are Henry, Liebert, and Boroson's regression lines for the SMC (*left*) and LMC (*right*). The two short horizontal solid bars on the right indicate median N/O for non–type I planetaries below $M_c = 0.8\ M_\odot$ (*upper*) and solar N/O (*lower*, labeled S). The vertical solid bar is the mean O/H for Population I planetaries.

reproduce (with their kind permission) Henry, Liebert, and Boroson's Figures 7*a* and 7*b* for the LMC and SMC, and overplot our Galactic data for type I nebulae. The Population I starting point, the median N/O for non–type I objects, and solar N/O are indicated by the labeled vertical and horizontal bars. Within rather wide limits, it is evident that our correlation for enriched nebulae parallels both of these. The offsets in both N/O and O/H are qualitatively similar to those found from H II regions (Dufour 1975; Pagel *et al.* 1978). It is also quite evident, given the initial Galactic values of type I nebulae of about log (N/O) ≈ -0.8 (solar) and log (O/H) + 12 $\approx$ 8.7 (Fig. 7) that the changes that take place in the LMC and SMC stars cum nebulae can be greater than in their Galactic counterparts.

From Torres-Peimbert (1983), the distribution of (N + O)/H versus N/O should be flat. We see by examination of Figure 7 that N/O $\approx$ 1 at O/H $\approx$ 4. As O/H drops to half, N/O about doubles. It is not clear whether oxygen is actually being destroyed or whether it is being diluted by a larger increase in nitrogen. We could examine the first possibility by looking at neon-to-oxygen ratios. Unfortunately, we do not have enough data to derive total neon abundances, and ionization correction factors are unreliable, so we have to make do with Ne^{+2} (Table 10), which provides only a lower limit. Nebulae that are at an optimal ionization level, for which most of the neon is in Ne^{+2}, should have Ne^{+2}/O values that approach 0.23 (Kaler 1978). Any that exceed this value would be candidates for oxygen depletion, since the neon abundance itself should change very little. We find only two nitrogen-enriched nebulae, K1-13 and M3-2, for which Ne^{+2}/O may be substantially elevated, at 0.30 and 0.26, respectively. The results are inconclusive. A large amount of neon data is needed, which includes reliable observations of other stages of ionization.

Whatever the explanation, it is clear that the dredge-up process as described by Becker and Iben (1979, 1980) is too feeble to produce the observed abundance alterations. Some form of hot bottom burning (Renzini and Voli 1981) is apparently required in order to reproduce the observed high nitrogen abundances. Whatever the answer, these composition changes provide a challenge to theory, and will ultimately tell us a great deal about stellar interior processes.

d) Evolutionary Time Scales

The theory of stellar evolution predicts the tracks that the stars must follow on the log *L*–log *T* plane as a function of core mass; it also gives the time it takes for a star of a given mass to reach a particular point in its development. In the case of the planetary nuceli, the matter involves the time elapsed since the star left the asymptotic giant branch (AGB). These ages can also be judged by the sizes of the nebulae by adopting measured expansion velocities or, in their absence, by assuming a mean expansion rate. Comparison of the two ages gives yet another way of adjudicating theory. Since the aging rates are expected to be a function of core mass, we should in principle be able to see an increase in the sizes of the nebulae as we proceed along an evolutionary track, and we should be able to see the nebular dimensions change as we shift from one track to another.

We approach the problem in two ways with different sets of evolutionary calculations, first by directly comparing observed and predicted nebular radii and then by comparing observed and theoretical correlations between the independently derived values of radius and central star temperature. We have estimated the time (hereafter, "evolutionary age") that each of the planetary nuclei in our sample has taken to evolve to its location on the log *L*–log *T* plane after exceeding log $T_{\rm eff} = 4.4$, according to the hydrogen-burning time scales used by Shaw (1989). Briefly, these time scales attempt to scale the ages calculated by Paczyński (1971) to those calculated by Schönberner (1979, 1981) and Iben (1984), who used superior evolutionary models. We can now use some data to test Shaw's (1989) theoretical distribution of stars on the log *L*–log *T* plane. More recent models by Wood and Faulkner (1986) show somewhat different time scales, but they cover a smaller range in core mass, and the published tables contain too few data to derive a reliable scaling to other core masses. The evolutionary ages were converted to predicted nebular radii (hereafter, "evolutionary radii") by assuming that the nebulae are ejected when they are first illuminated (i.e., at log $T_{\rm eff} = 4.4$) and that they expand at a constant rate of 20 km s^{-1}. Phillips (1989) gives a mean of 26 km s^{-1} for nebulae between 0.1 and 0.6 pc, and from Sabbadin (1984), Sabbadin, Ortolani, and Bianchini (1985), and Sabbadin, Strafella, and Bianchini (1986) we find a mean [O III] expansion velocity for 27 of our objects (including those from K83) of 24 km s^{-1}, consistent with the adopted canonical rate. (Obviously, they are ejected at about the time their central stars leave the AGB, but an error in the zero point of one or two thousand years makes no practical difference for this analysis; larger potential errors will be discussed below.) These evolutionary radii are plotted against the corresponding observed radii in Figure 10. Limits are shown with arrows, and points taken from other sources in the literature are denoted

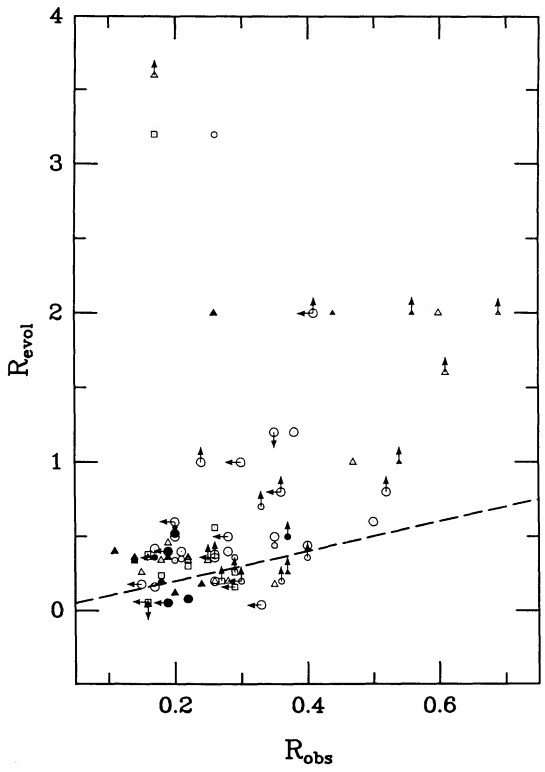

FIG. 10.—Observed nebular radius vs. that predicted from stellar evolution theory (both in parsecs), assuming a constant nebular expansion velocity of 20 km s^{-1}. Solid symbols denote those nebulae known to have faint outer halos, and smaller symbols denote those nebulae with approximate Hβ fluxes (see text). *Circles*: data from this study; *squares*: Hβ fluxes determined from radio data; *triangles*: data from Kaler (1983); *dashed line*: 1:1 relation.

with triangles; the one-to-one relation is shown as a dashed line.

While there appears to be some qualitative agreement, in general the evolutionary radii exceed those observed, sometimes greatly. (A few points that lie above the top of this figure are not shown.) A general trend of this sort could be remedied by assuming a different expansion velocity and/or an evolutionary age larger than zero at $t = 0$. One could even argue that the expansion velocity changes with time, particularly if a post–AGB stellar wind plays an important role in shaping the surrounding nebula itself at early times (see, e.g., Balick 1987; Dopita *et al.* 1987). However, points that differ greatly from the general trend require another explanation, the first obvious one being that we have neglected, or have not detected, the outermost faint halos that are evident in at least half of all planetary nebulae (Chu, Jacoby, and Arendt 1987). While a larger angular radius would, on the basis of the Shlovsky technique, also imply a larger distance, it could be argued that the Shklovsky distance really applies to that part of the nebula within which a specified mass of ionized nebular gas is contained, i.e., the "Shklovsky scale factor." Thus, if the faint outer halos contain very little mass, or if the bright, inner nebulae contain a mass equal to that adopted for the scale factor, then the inferred distances should be based upon the bright inner shells, and it is the outer radii that should be compared with those predicted from evolutionry time scales. The effect in Figure 10 would be to move many of the points to the right. Those with known outer shells are denoted with solid symbols.

There may be other explanations for the scatter in Figure 10 as well. In particular, the dynamical age of the nebula when it can first be ionized by its central star varies greatly—from nearly zero to more than 10^4 yr—depending largely upon the sizes of the hydrogen- and helium-rich shells that surround the carbon-oxygen core when the star evolves away from the AGB (Iben and Renzini 1983; Wood and Faulkner 1986). The range of this transition time (t_{tr}) from the AGB to the planetary nebula stage also decreases with increasing core mass. On the other hand, the nebular expansion rate itself may increase with core mass, since both the amount and the rate of change in ionizing flux (and, by implication, wind strength) is far greater for larger core masses. To probe these points, we plot in Figure 11 the ratio of the evolutionary to the observed nebular radii as a function of central star mass (the symbols are as in Fig. 10). Aside from a few outlying points that could not be plotted on this scale, and some to the upper right, there is a fairly clear correlation from upper left down and to the right. The plot shows that for low core mass the evolutionary radii can greatly exceed those observed, but that the trend declines and even reverses with increasing core mass. The decline in the vertical dispersion with increasing core mass could be understood in terms of a similar decline in the range of t_{tr} with increasing core mass. One interpretation of these plots is that the true rate of evolution is systematically faster than is predicted by the Schönberner/Iben time scales for lower mass planetary nuclei, and slower for those of higher mass. It is difficult to determine from these data which time scales need to be adjusted, since the dynamical age of the nebula is an imprecise absolute indicator of evolutionary age.

We next examine the subject from a different point of view in Figure 12, where we plot nebular radius against stellar temperature. The advantage of this procedure is that we compare two parameters that are observationally derived completely independently of one another. In the figure, temperature is

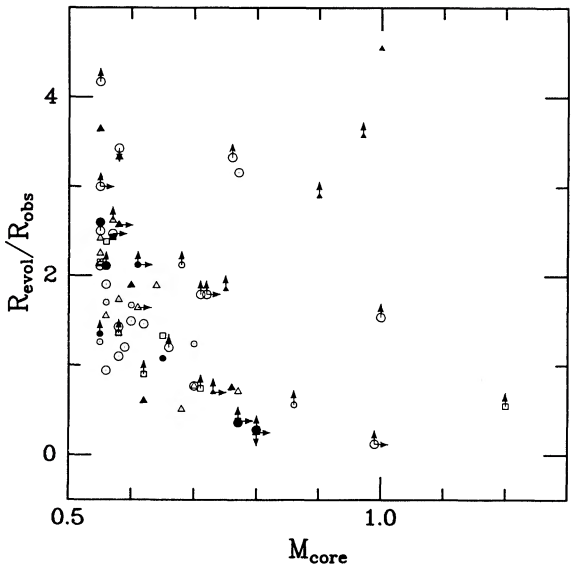

FIG. 11.—Ratio of predicted to observed nebular radius plotted against central star mass in solar units. Symbols are as in Fig. 10.

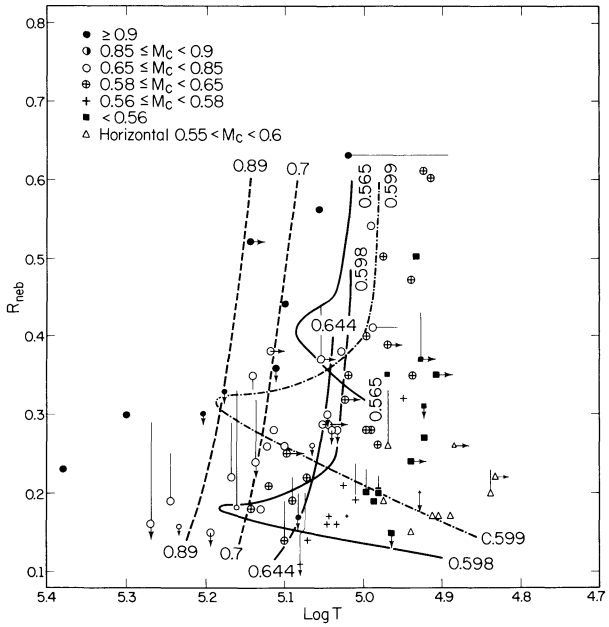

FIG. 12.—Nebular radius plotted against stellar effective temperature. All stars except for those represented by triangles are on cooling tracks. *Filled circles*: core mass from Wood and Faulkner (1986), and for higher mass from Paczyński (1971), $M_c \geq 0.9\ M_\odot$; *open circles*: $0.85 > Mc \geq 0.65\ M_\odot$; *circles with plus signs*: $0.65 > M_c \geq 0.58\ M_\odot$; *plus signs*: $0.58 > M_c \geq 0.56\ M_\odot$; *filled squares*: $M_c < 0.56\ M_\odot$; *triangles*: stars on the horizontal tracks; *smaller symbols*: M_c from crossover temperatures and as derived from surface brightness fluxes. *Solid lines*: theoretical curves labeled for different masses as derived from Schönberner (1981), where we assume an expansion velocity of 20 km s^{-1}; *dash-dot line*: theoretical curve from Iben (1984) for a 0.599 $M_\odot$ H-burning core and an expansion velocity of 20 km s^{-1}; *dashed lines*: theoretical curves from Wood and Faulkner (1986), also for an expansion velocity of 20 km s^{-1}, type A mass loss, and $\phi = 0.5$, where each curve is labeled with core mass.

directed to the right toward lower values as it is on the log L–log T plane. We divide the log L–log T plane (Fig. 5) into strips parallel to the descending (cooling) evolutionary tracks, and plot the stars symbolically according to core mass (in solar

masses): >0.9 (*closed circles*); $0.85 > M_c \geq 0.65$ (*open circles*); $0.65 > M_c \geq 0.58$ (*plus signs within circles*); $0.58 > M_c \geq 0.56$ (*plus signs*); and $M_c < 0.56$ (*filled squares*). Stars near the turnaround are treated as descending. The few stars that we include that are on horizontal (heating) tracks are denoted by triangles. Stars whose temperatures are derived from the crossover method are denoted by smaller symbols.

The figure shows just what we would expect: as the stars cool, the nebulae grow larger. The correlations are generally smooth and monotonic. The higher mass cores are shifted very clearly to the left, and the lower mass to the right, i.e., the nebulae grow progressively larger as the stars increase in mass and drop in luminosity along a line of constant temperature. The implication is that as long as nebular expansion velocities do not depend on core mass, it takes longer for a high-mass core to cool to a specific temperature than it does one of lower mass. Alternatively, it is possible that nebulae that develop from higher mass stars have higher expansion velocities, and simply grow larger after a given specific time. We have compared the expansion velocities from the sources cited above with both radius and core mass, and find no significant relationships. More expansion velocities at the high extremes of these two parameters are needed for a definitive answer, however. Given possible accelerations of the outbound gas by winds, and the decelerations produced by braking against the interstellar medium, it would be hard to know the relevance of current expansion velocities anyway. We consider the first scenario to be correct: the higher mass cores age (as measured by their descent time to log $T = 5.0$ or 4.9) more slowly. Clearly, however, much more work needs to be done on the expansion velocities. Finally, note that the few nebulae whose stars are still evolving to the left on the horizontal tracks are still small, as expected.

Now we fit the theory to the data, targeting some specific evolutionary tracks, where we use the predicted ages for a given log T and assume a standard expansion velocity of 20 km s^{-1} to calculate a nebular radius. First, we plot the data from the 0.599 $M_\odot$ hydrogen-burning core calculated by Iben (1984) as a dash-dot curve. The part that climbs up and to the left corresponds to the horizontal heating portion of the evolutionary track, and the part that goes up and to the right corresponds to the cooling portion. The curve passes nicely through the triangles—those on the heating track—but then goes vastly too far to the left, the theory aging the stars much too slowly, allowing the nebulae to grow much too large. Then on the cooling track it catches up to the points that represent the 0.6 $M_\odot$ stars before shooting upward too quickly, again aging the stars too slowly. The 0.5907 $M_\odot$ helium-burning curve (not shown) fits much more poorly, aging the stars even more lethargically.

Next, we plot the curves for 0.565, 0.598, and 0.644 $M_\odot$ from Schönberner (1981, 1989) as labeled solid lines. The behavior of the 0.598 $M_\odot$ curve is similar to Iben's, except that the turnover occurs at lower radius, allowing for a better fit. However, it then climbs much too rapidly again. The 0.565 $M_\odot$ curve clearly shows considerably too slow a pace, while the 0.644 curve just crosses its appropriate points at relatively low radius before again shooting rapidly upward. For higher radius, at least, the 0.644 and 0.598 $M_\odot$ curves are properly shifted relative to one another, that is, for higher masses the theory properly predicts that larger masses age the more slowly.

Finally, we plot as dashed lines the paths calculated from Wood and Faulkner's (1986) fading times. They present a complex set of evolutionary tracks in which they vary not only core mass but also the phase (ϕ) in the helium flash cycle at which the nebula was ejected, as well as the type of mass loss suffered by the nucleus (type A: mass loss cut off when the star leaves the AGB; type B: mass loss extended until the surface hydrogen content is reduced to 10^{-4} $M_\odot$). We choose $\phi = 0.5$ and type A mass loss, as they generally produce the lowest temperature curves (maximum rightward placement). The 0.76 $M_\odot$ curve falls practically atop the 0.7 $M_\odot$ curve and is not plotted. First, look at the two higher mass curves for $M_c \geq 0.70$ $M_\odot$. We clearly see that the shift to changing core mass is still correct (higher masses age more slowly to a given temperature), but again that the absolute placements of the curves are not satisfactory and that their slopes are much too high. Examine particularly the open circles (for which M_c is between 0.65 and 0.85 $M_\odot$) and compare them with the predicted 0.7 $M_\odot$ locus. The observed and predicted paths cross at a radius of about 0.2 pc, that is, the theory ages the stars first too rapidly and then too slowly. The time grid for the 0.6 $M_\odot$ track is too coarse to allow placement of its curve in Figure 12. The difference between a star that is released as a helium burner ($\phi = 0$) and one that burns only hydrogen is too small to allow discrimination.

There are several serious and valid criticisms that can be leveled at these analyses. Aside from observational uncertainties such as the distance scale, limiting stellar temperatures and luminosities, undetected faint nebular halos, and so on, there are many conceptual problems. The most serious is that we do not know *a priori* whether the luminosity for any given central star is provided mostly by hydrogen or by helium-shell burning. It is clear from the evolutionary models (e.g., Iben and Renzini 1983; Wood and Faulkner 1986; Iben and Tutukov 1989) that the path of a planetary core through the log L–log T plane, as well as the rate of evolution, is substantially different for different sources of luminosity. Thus, if any of the stars in our sample are powered by helium-shell burning, then both the core mass and the evolutionary age are incorrect—the latter by a factor of perhaps 3 or more. While one could speculate about what evolutionary track a given nucleus is following, the relevant data are scarce and in any case would probably not be definitive.

There are other problems with our approach as well. First, nebular shells may well not expand at a constant velocity near 20 km s^{-1}, particularly during the early portion of their evolution at constant luminosity when the stellar wind is likely to be strongest. It seems likely that the angular size of a young nebula will be a function both of the central star's luminosity and of the time spent at that luminosity once log $T_{\rm eff} = 4.4$ has been exceeded. If this is the case, then our inferred dynamical ages for younger nebulae will be incorrect by an amount that depends upon core mass. Second, the expansion of older nebulae may be slowed by the interstellar medium. We also cannot be certain whether a given nucleus has been "born again," i.e., whether it has suffered a post–AGB shell flash and cycled back through the planetary nebula portion of the log L–log T plane (Iben *et al.* 1983). While this possibility is thought to be rare, it is yet another opportunity for a discrepancy between the dynamical and evolutionary ages to be misinterpreted. In addition, even small errors in the estimation of stellar luminosity or temperature can sometimes lead to large errors in the inferred evolutionary age. Thus, a scatter in the evolutionary radii of a factor of 2 might be expected.

Finally, the distances and radii are subject to significant

error. The Shklovsky scale factor, once again, may be larger (e.g., Cudworth 1974), as supported by Méndez *et al.* (1988), which would raise all the radii by a factor of 1.45 and decrease the core masses by an inconstant multiplier (about 0.1 $M_\odot$ at 0.76 $M_\odot$: see Fig. 5). The result would be that the observed points would be systematically higher above the theoretical curves, and it would be more correct to say that over the observed range of planetaries the theory ages the stars too rapidly. Another possibility is that the scale factor could be a function of core mass (§ IV*b*), leading to systematic error in the stellar luminosity and consequently in the evolutionary radii. However, this explanation is unlikely to come close to curing all the offsets and slope differences. Nevertheless, even with all the problems, we demonstrate remarkable internal consistency between the evolution of the stars and that of the nebulae. The implication is that the luminosities are at least *relatively* correct as derived by the Shklovsky distance and Zanstra methods.

Our results are in some accord with those derived by McCarthy *et al.* (1990), though we have only one object (NGC 7293) in common. Most of theirs are on horizontal or heating evolutionary tracks, whereas ours are mostly on cooling or descending tracks. They employ stellar spectroscopy to derive temperature and surface gravity independently of distance, whereas we use nebular photometry dependent upon statistical assumptions of distance to derive temperature and luminosity. The temperatures they derive are generally lower than those found by the Zanstra method (Méndez *et al.* 1988; Kaler 1989), and the distances are considerably larger than those found by the Shklovsky method (compare Méndez *et al.* 1988; Daub 1982; K83; see also McCarthy *et al.* 1990). Figure 1 of McCarthy *et al.* (1990) (which is displayed as ages rather than radii) bears some resemblance to our Figure 10. The big difference is that for small objects their dynamical ages (radii) are considerably larger than the evolutionary ages, whereas at 0.15–0.20 pc or so ours tend to agreement. Part of that is due to the larger distance scale that they use, and part to the use of different evolutionary tracks. However as the nebulae grow, the dynamical age becomes smaller than the evolutionary; that is, the systematic trends are the same. The agreement is better with our Figure 12, which shows the nebulae at first too large relative to the theoretical loci, and then too small. Unfortunately, their reversal is based upon only three nebulae. McCarthy *et al.* (1990) suggest that when the dynamical age is the larger, it is because the evolutionary age is too small (i.e., evolution is too rapid) as a result of too little residual envelope mass, which makes the crossing time from the end of the superwind phase to the onset of nebular ionization too short. The dynamical age is shorter only when the wind continues past the theoretically assumed stopping point, which they suggest happens for lower mass cores. Thus we would expect to see that lower mass cores might be the ones to evolve more quickly. However, in our work we see that the observed points cross over the Wood and Faulkner (1986) theoretical curves at all masses above 0.6 $M_\odot$, that is, the reversal between dynamical and evolutionary age is more mass-independent.

Considering all of the difficulties we encounter in our analysis, it is somewhat surprising that there are such striking correlations between observational parameters and—even with the various discrepancies—between the observed and evolutionary nebular radii. Our interpretation is that many, if not most, of the central stars are, in fact, following the hydrogen-burning tracks. The range in T_{tr} does seem to decline with increasing core mass, and higher mass stars age to a given temperature more quickly also with increasing mass as predicted by theory. However, it is patently clear that, at least for cooling stars, the predicted rates of evolution do not follow well the rate observed; for example, the most recent, from Wood and Faulkner (1986), are too fast at higher luminosity and temperature and too slow at lower. The nebulae whose central stars do not follow the general trends evident in the figures may also be candidates for one of (1) an undetected outer nebular halo, (2) a central star that is following a helium-burning evolutionary track and/or that may have suffered a post–AGB thermal pulse, or (3) a very poorly determined distance or, in a few cases, even stellar temperature. What are badly needed now are improved observational samples and reconciliation of the distance and temperature determinations derived from nebular and stellar analyses. Whatever the outcome, it is clear from both works that the current theories of stellar evolution do not produce the correct stellar ages.

V. CONCLUSIONS

Our summary view is that theory is approaching an explanation of the way by which planetary nebulae and their nuclei develop and evolve, but that it is still rather wide of the mark. One major reason is that there have been insufficient accurate data on which to base such theory. This paper alleviates a serious problem of observational selection, since it concentrates on larger nebulae whose distances can be more accurately defined and whose core masses are systematically larger.

We show that the N/O versus He/H relation may follow more than one path as a function of mass, and more particularly that ordinary dredge-up processes (without additional burning) cannot match the high nitrogen and helium compositions observed. More important, we define an actual relation between nitrogen enrichment and core mass, providing better data on which to base an improved theory. The data support the likelihood of envelope burning, at least for intermediate-mass stars. We also confirm and define the depletion, or drop, in O/H for type I nebulae as N/O increases, such that (N + O)/H remains fairly constant.

Finally, we clearly tie stellar and nebular evolution together by correlating the observed and theoretical radii, and by correlating the nebular radii with stellar core masses and effective temperatures. We show that the theory fits qualitatively but not quantitatively. Although there is usually a radius at which the theoretical and kinematic ages agree, the stars of the large nebulae are in general predicted to age first too rapidly and then too slowly as they descend to the white dwarfs (the point of crossover depending on the distance scale). The work here provides additional data on which to base future theoretical developments in the evolution of post–AGB stars.

This research was supported by the National Science Foundation through grants NSF AST 84-19355 and 88-13686 to the University of Illinois and NSF AST 84-14827 to Williams College. J. B. K. would also like to thank the administration of the University of Illinois Center for Advanced Study for their additional support, and the University of Illinois Research Board for an allocation of computer time. K. S. K. also acknowledges support from a William and Flora Hewlet Foundation grant of Research Corporation. In addition, we would like to thank the staffs of Kitt Peak National Observatory and Steward Observatory for their assistance, Walter Kailey for assistance in observing and in data reduction, and Louise Browning for assistance in data measurement and in proofreading.

REFERENCES

Abell, G. O. 1966, *Ap. J.*, **144**, 259.
Aller, L. H. 1983, in *IAU Symposium 103, Planetary Nebulae*, ed. D. R. Flower (Dordrecht: Reidel), p. 1.
Aller, L. H., and Czyzak, S. J. 1978, *Proc. Nat. Acad. Sci.*, **75**, 1.
———. 1979, *Ap. Space Sci.*, **62**, 397.
———. 1983, *Ap. J. Suppl.*, **51**, 211.
Aller, L. H., and Keyes, C. D. 1987, *Ap. J. Suppl.*, **65**, 405.
Balick, B. 1987, *A.J.*, **94**, 671.
Barker, T. 1980, *Ap. J.*, **240**, 99.
———. 1984, *Ap. J.*, **284**, 589.
Becker, S. A., and Iben, I., Jr. 1979, *Ap. J.*, **232**, 831.
———. 1980, *Ap. J.*, **237**, 111.
Brocklehurst, M. 1971, *M.N.R.A.S.*, **153**, 471.
Brown, A., and Mathews, W. 1970, *Ap. J.*, **160**, 939.
Cahn, J. H., and Kaler, J. B. 1971, *Ap. J. Suppl.*, **22**, 319.
Chu, Y.-H., Jacoby, G. H., and Arendt, R. 1987, *Ap. J. Suppl.*, **64**, 529.
Chu, Y.-H., Kwitter, K. B., Kaler, J. B., and Jacoby, G. H. 1984, *Pub. A.S.P.*, **96**, 598.
Clegg, R. E. S. 1987, *M.N.R.A.S.*, **229**, 31P.
Cudworth, K. M. 1973, *Pub. A.S.P.*, **85**, 401.
———. 1974, *A.J.*, **79**, 1384.
Daub, C. T. 1982, *Ap. J.*, **260**, 612.
Dengel, J., Hartl, H., and Weinberger, R. 1980, *Astr. Ap.*, **85**, 356.
Dopita, M. A., Meatheringham, S. J., Wood, P. R., Webster, B. L., Morgan, D. H., and Ford, H. C. 1987, *Ap. J. (Letters)*, **315**, L107.
Dufour, R. J. 1975, *Ap. J.*, **195**, 315.
———. 1984, *Ap. J.*, **287**, 341.
Gutiérrez-Moreno, A., Moreno, H., and Cortés, G. 1985, *Pub. A.S.P.*, **97**, 397.
Hawley, S. A. 1978, *Pub. A.S.P.*, **90**, 370.
Hayes, D. S. 1970, *Ap. J.*, **159**, 165.
Heap, S. R., and Hintzen, P. M. 1989, *Ap. J.*, **353**, 200.
Henry, R. B. C., Liebert, J., and Boroson, T. A. 1989, *Ap. J.*, **339**, 872.
Henry, R. B. C., and Shipman, H. L. 1986, *Ap. J.*, **311**, 774.
Iben, I., Jr. 1984, *Ap. J.*, **277**, 333.
Iben, I., Jr., Kaler, J. B., Truran, J. W., and Renzini, A. 1983, *Ap. J.*, **264**, 605.
Iben, I., Jr., and Renzini, A. 1983, *Ann. Rev. Astr. Ap.*, **21**, 271.
Iben, I., Jr., and Truran, J. W. 1978, *Ap. J.*, **220**, 980.
Iben, I., Jr., and Tutukov, A. 1989, *Ap. J.*, **342**, 430.
Jacoby, G. H. 1988, private communication.
Jacoby, G. H., and Kaler, J. B. 1989, *A.J.*, **98**, 1662.
Kaler, J. B. 1976, *Ap. J. Suppl.*, **31**, 517.
———. 1978, *Ap. J.*, **225**, 527.
———. 1980, *Ap. J.*, **239**, 78.
———. 1981, *Ap. J. (Letters)*, **250**, L31.
———. 1983, *Ap. J.*, **271**, 188 (K83).
———. 1985*a*, *Ap. J.*, **290**, 531.
———. 1985*b*, *Ann. Rev. Astr. Ap.*, **23**, 89.
———. 1986, *Ap. J.*, **308**, 322.
———. 1989, in *IAU Symposium 131, Planetary Nebulae*, ed. S. Torres-Peimbert (Dordrecht: Kluwer), p. 229.
Kaler, J. B., Chu, Y.-H., and Jacoby, G. H. 1988, *A.J.*, **96**, 1407.
Kaler, J. B., and Feibelman, W. A. 1985, *Ap. J.*, **297**, 724.
Kaler, J. B., and Jacoby, G. H. 1989, *Ap. J.*, **345**, 871.
Kaler, J. B., and Shaw, R. A. 1984, *Ap. J.*, **278**, 195.
Koester, D., Schulz, H., and Weidemann, V. 1979, *Astr. Ap.*, **76**, 262.
Koutek, L. 1971, *Astr. Ap.*, **13**, 493.
———. 1972, *Astr. Ap.*, **16**, 291.
Kwitter, K. B., and Jacoby, G. H. 1989, *A.J.*, **98**, 2159.
Kwitter, K. B., Jacoby, G. H., and Lawrie, N. G. 1983, *Pub. A.S.P.*, **95**, 732.
Kwitter, K. B., Jacoby, G. H., and Lydon, T. J. 1988, *A.J.*, **96**, 997.
Kwok, S. 1983, in *IAU Symposium 103, Planetary Nebulae*, ed. D. R. Flower (Dordrecht: Reidel), p. 293.
Longmore, A. J. 1977, *M.N.R.A.S.*, **178**, 251.
Longmore, A. J., and Tritton, S. B. 1980, *M.N.R.A.S.*, **193**, 581.
McCarthy, J. K., Mould, J. R., Méndez, R. H., Kudritzki, R. P., Husfeld, D., Herrero, A., and Groth, H. G. 1990, *Ap. J.*, **351**, 230.
Méndez, R. H., Kudritzki, R. P., Herrero, A., Husfeld, D., and Groth, H. G. 1988, *Astr. Ap.*, **190**, 113.
Milne, D. K. 1979, *Astr. Ap. Suppl.*, **36**, 227.
Milne, D. K., and Aller, L. H. 1982, *Astr. Ap. Suppl.*, **50**, 209.
O'Dell, C. R. 1963, *Ap. J.*, **138**, 293.
Oke, J. B. 1974, *Ap. J. Suppl.*, **27**, 21.
Oke, J. B., and Schild, R. E. 1970, *Ap. J.*, **161**, 1015.
Oster, L. 1961, *Ap. J.*, **134**, 1010.
Paczyński, B. 1971, *Acta Astr.*, **21**, 417.
Pagel, B. E. J., Edmunds, M. G., Fosbury, R. A. E., and Webster, B. L. 1978, *M.N.R.A.S.*, **184**, 569.
Peimbert, M. 1978, in *IAU Symposium 76, Planetary Nebulae*, ed. Y. Terzian (Dordrecht: Reidel), p. 215.
Peimbert, M., and Serrano, A. 1980, *Rev. Mexicana Astr. Af.*, **5**, 9.
Peimbert, M., and Torres-Peimbert, S. 1983, in *IAU Symposium 103, Planetary Nebulae*, ed. D. R. Flower (Dordrecht: Reidel), p. 233.
———. 1987, *Rev. Mexicano Astr. Af.*, **14**, 540.
Perek, L. 1971, *Bull. Astr. Inst. Czechoslovakia*, **22**, 103.
Perek, L., and Koutek, L. 1967, *Catalogue of Galactic Planetary Nebulae* (Prague: Czechoslovak Academy of Sciences).
Phillips, J. B. 1989, in *IAU Symposium 103, Planetary Nebulae*, ed. S. Torres-Peimbert (Dordrecht: Kluwer), p. 425.
Purgathofer, A. 1978, *Astr. Ap.*, **70**, 589.
Purgathofer, A., and Weinberger, R. 1980, *Astr. Ap.*, **87**, L5.
Renzini, A. 1979, in *Proc. Fourth IAU European Regional Meeting, Astronomy, Stars and Star Systems*, ed. B. E. Westerlund (Dordrecht: Reidel), p. 155.
Renzini, A., and Voli, M. 1981, *Astr. Ap.*, **94**, 175.
Ross, J. A., and Aller, L. H. 1976, *Science*, **191**, 1223.
Sabbadin, F. 1984, *Astr. Ap. Suppl.*, **58**, 273.
Sabbadin, F., Ortolani, S., and Bianchini, A. 1985, *M.N.R.A.S.*, **213**, 563.
Sabbadin, F., Strafella, F., and Bianchini, A. 1986, *Astr. Ap. Suppl.*, **65**, 259.
Schneider, S. E., Terzian, Y., Purgathofer, A., and Perinotto, M. 1983, *Ap. J. Suppl.*, **52**, 399.
Schönberner, D. 1979, *Astr. Ap.*, **79**, 108.
———. 1981, *Astr. Ap.*, **103**, 119.
———. 1989, in *IAU Symposium 131, Planetary Nebulae*, ed. S. D. Torres-Peimbert (Dordrecht: Kluwer), p. 463.
Schönberner, D., and Weidemann, V. 1981, private communication.
Seaton, M. J. 1960, *Rept. Progr. Phys.*, **23**, 313.
———. 1968, *M.N.R.A.S.*, **139**, 129.
Shao, C.-Y., and Liller, W. 1973, private communication.
Shaw, R. A. 1989, *IAU Symposium 131, Planetary Nebulae*, ed. S. Torres-Peimbert (Dordrecht: Kluwer), p. 473.
Shaw, R. A., and Kaler, J. B. 1985, *Ap. J.*, **295**, 537.
———. 1989, *Ap. J. Suppl.*, **69**, 495.
Stone, R. P. S. 1977, *Ap. J.*, **218**, 767.
Torres-Peimbert, S. 1983, in *Stellar Nucleosynthesis* (*Ap. Space Sci. Lib.*, Vol. **109**), ed. C. Chiosi and A. Renzini (Dordrecht: Reidel), p. 3.
Torres-Peimbert, S., and Peimbert, M. 1978, *Rev. Mexicana Astr. Af.*, **2**, 181.
———. 1987, *Rev. Mexicana Astr. Af.*, **14**, 540.
Weinberger, R. 1977, *Astr. Ap. Suppl.*, **30**, 343.
Whitford, A. E. 1958, *A.J.*, **63**, 201.
Wood, P. R., and Faulkner, D. J. 1986, *Ap. J.*, **307**, 659.
Zylastra, A., Pottasch, S. R., and Bignell, C. 1989, *Astr. Ap. Suppl.*, **79**, 329.

JAMES B. KALER: Department of Astronomy, University of Illinois, 103 Astronomy Building, 1002 West Green, Urbana, IL 61801

KAREN B. KWITTER: Department of Astronomy, Thomson Physics Laboratory, Williams College, Williamstown, MA 01267

RICHARD A. SHAW: Computer Sciences Corporation, NASA/Goddard Space Flight Center, Code 684.9, Greenbelt, MD 20771